IV Escola de Primavera de Transição e Turbulência
Universidade Federal do Rio Grande do Sul
Pontifícia Universidade Católica do Rio Grande do Sul
Porto Alegre, RS, 27 de setembro a 1º de outubro de 2004

INDUSTRIAL AEROACOUSTICS: EXCITATION MECHANISMS AND COUNTER-MEASURES

Samir Ziada
McMaster University
Hamilton, Ontario, L8S 4L7
Canada
ziadas@mcmaster.ca

Many noise and vibration problems in industry are generated by excitation mechanisms involving the coupling between a flow instability and an upstream feedback. In the fluid-dynamic mechanism, the upstream feedback is generated by the flow impingement on a downstream solid object, whereas in the fluid-resonant and the fluid-elastic mechanisms, this feedback is generated by acoustic or structural resonances of the associated system. This paper focuses on the fluid-dynamic and the fluid-resonant mechanisms; describing their basic features and means of their alleviation. As an example of the fluid-resonant mechanism, acoustic resonances of closed side-branches are discussed in some detail; including the effect of flow and geometrical parameters, the prediction of the onset of resonance, estimation of the resonance intensity as well as practical means of reducing the resonance intensity or eliminating it altogether.

Key words: Impinging flow, fluid-dynamic mechanism, fluid-resonant mechanism, acoustic resonance, closed side-branches, feedback control

1. Introduction

Fluid flows in many engineering applications are naturally unstable. This means that small disturbances to the flow can be amplified into large vortex-like structures which generate fluctuating fluid forces and noise. Numerous theoretical and experimental studies have improved our knowledge of how flow instabilities develop in regions of wall bounded and separated shear flows such as, boundary layers, free shear layers, wakes of bluff bodies or free jets. A comprehensive review of recent advances in the field of flow instabilities has been published by Huerre & Monkewitz (1990). When an unstable flow interacts with either the vibration of a nearby flexible structure or with the sound waves generated by acoustic resonances, a feedback excitation mechanism is initiated which strengthens drastically the structural vibration and the generated noise. As an example of the feedback mechanism between flow instabilities and sound waves, the pleasant tones of the flute are produced by the coupling between the instability of the air stream being blown and the sound waves inside the flute "pipe".

Unfortunately, when this coupling mechanism becomes active in industrial applications, such as power stations, chemical plants, gas and oil pipelines, or marine and aeronautical applications, the outcome is not as pleasant as in the case of the flute but rather, deafening noise levels, dangerous excessive vibrations, and a large amount of wasted energy can result. This makes the environment at the work place and in neighbouring communities intolerable, the safety of the plant is endangered in cases of failure due to vibrations, and the efficiency of the industrial process is lowered. Additionally, the financial consequences can be devastating if a plant is put out of service to carry out repairs or because of safety or environmental concerns. An unscheduled shut-down of a 400 MW power plant, for example, results in lost revenues of around half a million dollar per day. Even when the vibration and pressure pulsation are sufficiently weak to be tolerated, they still cause

additional pressure losses and reduce the efficiency. *However small these losses might seem in percentage terms, they constitute, in absolute values, a significant amount of wasted energy.*

The object of this paper is to describe the instability of separated shear flows and its various coupling mechanisms with sound waves, which result in the generation of excessive noise and/or dangerous vibration in a wide range of industrial applications. Passive and active control methods to suppress these coupling mechanisms are also addressed in some details. As an example, the excitation mechanism causing acoustic resonances of closed side-branches is discussed and several means to alleviate these resonances are described.

2. Excitation Mechanisms Due to Instability of Shear Flows

Free shear flows, such as wakes of bluff bodies, free shear layers and free jets, see Fig. (2.1), are inherently unstable and therefore small disturbances introduced near the location of flow separation are rapidly amplified downstream into vortex-like structures. The growth and downstream convection of these vortical structures generates pressure and velocity fluctuations, which appear in the turbulence and pressure spectra as a discrete frequency excitation, whose frequency varies linearly with the flow velocity. This excitation is generally referred to in the literature as Strouhal excitation or vorticity shedding.

In turbulent flow, which is likely to be the prevalent case in practical applications, vorticity shedding resulting from shear flow instabilities is normally incoherent and therefore its excitation level is generally weak, *unless it is coupled with a feedback mechanism, which perpetuates the inducement of coherent disturbances near the location of flow separation*. When this occurs, the flow oscillations are drastically enhanced such that excessive vibration and/or acute noise problems are likely to occur.

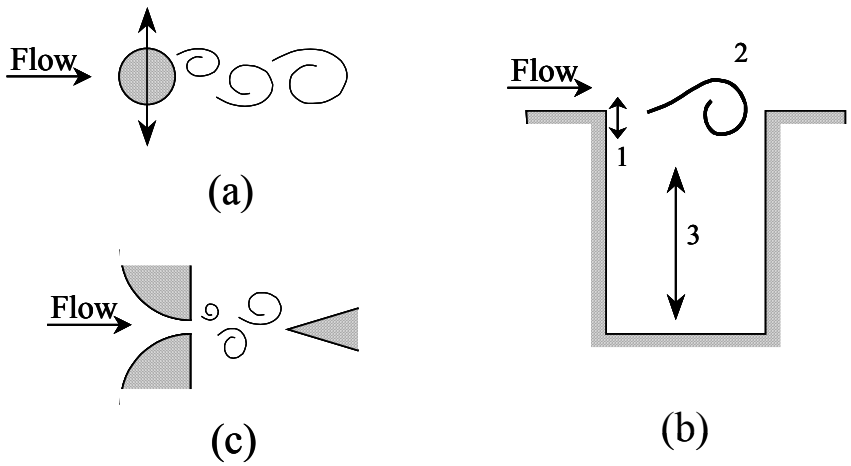

Figure 2.1. Basic feedback mechanisms which enhance shear flow excitations: (a) feedback due to the "locked-in" vibration of the cylinder; (b) new vorticity perturbations (1) are induced by the resonant acoustic standing waves (3) which are excited by the shear layer oscillation (2); (c) feedback is due to flow impingement on the wedge.

Basically, there are three different mechanisms which generate upstream feedback of disturbance (Rockwell & Naudascher, 1979). In the first, the feedback is provided by structural vibrations as in the classical case of vortex shedding from flexible bluff bodies, Fig. (2.1(a)). This mechanism can generate large amplitude, or 'lock-in' vibration when the vortex shedding frequency approaches the resonance frequency of the bluff body. The second mechanism, *the fluid-resonant*

mechanism, is triggered when the frequency of vorticity shedding becomes close to that of an acoustic resonator. In this case, acoustic feedback is provided by the resonant sound field as in the classical cases of deep cavity resonance, Fig. (2.1(b)), and acoustic resonance of conduits due to vortex shedding from bluff bodies, Fig. (2.2). In the third mechanism, *the fluid-dynamic mechanism*, upstream feedback is not caused by resonance effects, but rather by flow impingement on a downstream object. The jet-edge oscillator shown in Fig. (2.1(c)) is a classical example of this feedback mechanism. The distortion of the vorticity field due to its impingement on the edge generates an upstream feedback, whereby new perturbations are induced at the jet exit. All three of the above mechanisms can coexist, albeit rarely, but when they do, the problem becomes very severe. Ziada and Bühlmann (1991), for example, reported a vibration problem for a long corrugated pipe conveying water, in which conditions conducive to the above three mechanisms existed: the shear layers spanning the corrugations troughs comprised impinging flow situation, the corrugations exhibited significant axial vibration and acoustic standing waves in the pipe were also observed. The excitation mechanism in this case is very complex and its details are not yet fully understood.

The contents of this paper are organized in the following manner. First, the hydrodynamic stability theory of free shear flows is discussed briefly. It is clear that full understanding of this phenomenon is essential because the flow instability is the source of excitation in all the above-mentioned mechanisms. Attention is then focused on the effect of shear flow impingement on downstream objects. The main features of the *fluid-dynamic* excitation mechanism which controls the oscillations of impinging shear flows are illustrated by means of several examples of impinging mixing layers and jets. Thereafter, the *fluid-resonant* excitation mechanism, which results from the interaction of flow instabilities and sound waves, is demonstrated with reference to the classical case of acoustic resonance of deep cavities.

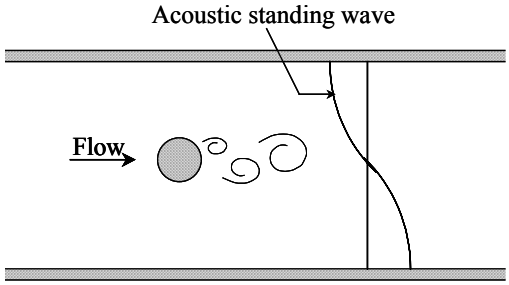

Figure 2.2. Vortex shedding from bluff bodies can excite acoustic standing waves in the transverse direction of the duct.

3. Hydrodynamic Stability Theory of Shear Flows

The general meaning of stability can be explained by asking the question: Can the system physical state endure a disturbance and still return to its original state? If yes, then it is stable. If not, then that particular state of the system is unstable. Thus, stability analysis consists of examining the effect of a disturbance, with a particular frequency, on a given state of the system. In this context, the following applies to fluid flows, and in particular to shear flows.

- Stability is the fluid quality of being immune to small disturbances. These disturbances can be either self-induced or externally imposed.

- The decay of an introduced small disturbance is the necessary condition for stability.

- The amplification factor (whether temporal or spatial) determines the rate at which an infinitesimally small disturbance, once introduced, will amplify or decay (with time, i.e. temporal amplification, or space, i.e. spatial amplification).

- The basic equation used to examine flow instability is a *perturbation* form of the Navier-Stokes equation (NSE).

- We are interested in finding out the flow response to *small* disturbances, which is representative of the *initial phase* of instability.

- If the perturbed NSE is linearized, we obtain the Orr-Sommerfeld equation. Neglecting viscous effects in the Orr-Sommerfeld equation gives the Rayleigh equation.

- Linear stability theory predicts the most unstable frequency of the disturbance (i.e. the frequency which has the largest amplification factor). This frequency dominates transition from laminar to turbulent regimes.

3.1. Derivation of the Orr-Sommerfeld equation

- Since previous work showed that R_{cr} (critical Reynolds number for transition) is lower and the amplification rate of disturbances is larger for 2-D flows than those for 3-D flows, we confine our analysis to two-dimensional flows. Thus, the 2-D analysis is conservative for three-dimensional flows.

- We assume a velocity disturbance function (also two-dimensional) and substitute in NSE and since the disturbance amplitude is very small at the initial phase, the equations are linearized by neglecting higher order terms.

- Viscous effects are neglected by assuming high Reynolds number.

- The resulting equation is then solved numerically (as an eigenvalue problem) to find:
  (a) The frequency range at which the flow is unstable
  (b) The amplification factor, phase speed, wave number as functions of disturbance frequency.

- Results of the linear stability theory are in good agreement with the experimental results taken in the initial region of transition, which is where the disturbance is still small.

The two dimensional NSE (without body forces) is written as:

$$\frac{\partial u}{\partial t} + u\frac{\partial u}{\partial x} + v\frac{\partial u}{\partial y} + \frac{1}{\rho}\frac{\partial p}{\partial x} = \nu\left(\frac{\partial^2 u}{\partial x^2} + \frac{\partial^2 u}{\partial y^2}\right) \tag{1}$$

$$\frac{\partial v}{\partial t} + u\frac{\partial v}{\partial x} + v\frac{\partial v}{\partial y} + \frac{1}{\rho}\frac{\partial p}{\partial y} = \nu\left(\frac{\partial^2 v}{\partial x^2} + \frac{\partial^2 v}{\partial y^2}\right) \tag{2}$$

The Continuity equation is

$$\frac{\partial u}{\partial x} + \frac{\partial v}{\partial y} = 0 \tag{3}$$

Where u & v are the velocity components in x & y directions, p is the pressure, ρ is the density and ν is the viscosity.

If we assume a two-dimensional parallel flow with a mean flow as shown, the velocity components are therefore

$$\left.\begin{array}{l} U(y), \quad V = W = 0 \\ \text{and} \quad P = P(x, y) \end{array}\right\} \tag{4}$$

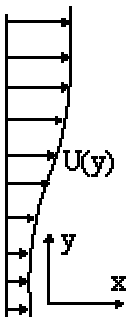

$$\frac{\partial u'}{\partial t} + U\frac{\partial u'}{\partial x} + v'\frac{\partial U}{\partial y} + \frac{1}{\rho}\frac{\partial P}{\partial x} + \frac{1}{\rho}\frac{\partial p'}{\partial x} = \nu\left(\frac{d^2U}{dy^2} + \nabla^2 u'\right)$$

Assume a two dimensional perturbation of the form

$$u'(x, y, t),\ v'(x, y, t),\ p'(x, y, t)\text{, and } w' = 0 \tag{5}$$

The resultant motion becomes

$$u = U(y) + u',\quad v = v',\quad w = 0,\quad p = P + p' \tag{6}$$

Substitute Eq. (6) into Eq. (1), Eq. (2) and Eq. (3) and neglecting second order terms

$$\frac{\partial u'}{\partial t} + U\frac{\partial u'}{\partial x} + v'\frac{\partial U}{\partial y} + \frac{1}{\rho}\frac{\partial P}{\partial x} + \frac{1}{\rho}\frac{\partial p'}{\partial x} = \nu\left(\frac{d^2U}{dy^2} + \nabla^2 u'\right) \tag{7}$$

$$\frac{\partial v'}{\partial t} + U\frac{\partial v'}{\partial x} + \frac{1}{\rho}\frac{\partial P}{\partial y} + \frac{1}{\rho}\frac{\partial p'}{\partial y} = \nu\nabla^2 v' \tag{8}$$

$$\frac{\partial u'}{\partial x} + \frac{\partial v'}{\partial y} = 0 \tag{9}$$

The mean flow (Eq. (4)) satisfies the NSE. Thus, substituting Eq. (4) into Eq. (1) and Eq. (2) and then canceling terms in Eq. (7) and Eq. (8), we obtain

$$\frac{\partial u'}{\partial t} + U\frac{\partial u'}{\partial x} + v'\frac{dU}{\partial y} + \frac{1}{\rho}\frac{\partial p'}{\partial x} = \nu\nabla^2 u' \tag{10a}$$

$$\frac{\partial v'}{\partial t} + U\frac{\partial v'}{\partial x} + \frac{1}{\rho}\frac{\partial p'}{\partial y} = \nu\nabla^2 v' \tag{10b}$$

Equations (10a & 10b) are the NSE for a small disturbance.

3.2. The Orr-Sommerfeld equation

The stream function of a two-dimensional, *harmonic* disturbance is

$$\overline{\psi}(x,y,t) = \overline{\varphi}(y)\, e^{j(\alpha x - \beta t)}$$
$$u' = \frac{\partial \overline{\psi}}{\partial y} = \frac{\partial \overline{\varphi}}{\partial y}\, e^{j(\alpha x - \beta t)}$$
$$v' = -\frac{\partial \overline{\psi}}{\partial x} = -\, j\alpha \overline{\varphi}\, e^{j(\alpha x - \beta t)}$$

β : dimensionless frequency

$C = \beta/\alpha$: phase speed (11)

where complex quantities are indicated by the over bar. Substituting into Eq. (10) and eliminating the pressure, we obtain a fourth order, differential equation for the complex amplitude of the disturbance function $\overline{\varphi}$

$$(U - C)\left(\frac{\partial^2 \overline{\varphi}}{\partial y^2} - \alpha^2 \overline{\varphi}\right) - \frac{\partial^2 U}{\partial y^2}\overline{\varphi} = -\frac{j}{\alpha R}\left(\frac{\partial^4 \overline{\varphi}}{\partial y^4} - 2\alpha^2 \frac{\partial^2 \overline{\varphi}}{\partial y^2} + \alpha^4 \overline{\varphi}\right) \tag{12}$$

This is the Orr-Sommerfeld equation and it is in a dimensionless form. Assuming high Reynolds number flows, the right-hand side of the equation can be neglected (since 1/R is small). Then we have the Rayleigh's equation.

$$(U - \overline{C})\left(\frac{\partial^2 \overline{\varphi}}{\partial y^2} - \overline{\alpha}^2 \overline{\varphi}\right) - \frac{\partial^2 U}{\partial y^2}\overline{\varphi} = 0 \tag{13}$$

Here, U and $\overline{\varphi}$ are functions of y. This equation is solved numerically for a given mean velocity distribution U(y).

For example, for the hyperbolic tangent velocity profile, which is shown in below, Michalke (1965) reported detailed instability characteristics for the profile

$$U(y) = 0.5\,(1 + \tanh y) \tag{14}$$

and with the boundary conditions

$$\text{at } y = \pm\infty \quad \rightarrow \quad \overline{\varphi} = 0$$

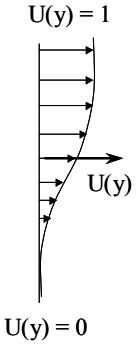

3.3. Temporal and spatial amplifications

Depending on the choice of α and C, real or imaginary, we may study the growth of the instability wave (i.e. disturbance) with either time (temporal amplification factor β_i) or with location (spatial amplification α_i).

(a) Temporal amplification: If $\overline{C}$ is complex and α is real, Eq. (11) gives:

$$\overline{\psi}(x, y, t) = \left\{\overline{\varphi}(y)\ e^{\beta_i t}\right\} e^{j(\alpha x - \beta_r t)} \tag{15}$$

The value in the brackets represents the time-dependent amplitude of a wave traveling in the x-direction with a frequency β_r and a wave number α. It is seen that for this amplitude to grow with time, i.e. for the flow to be unstable, β_i must be positive ($\beta_i > 0$).

(b) Spatial amplification: When C is real and $\overline{\alpha}$ is complex, Eq. (11) gives:

$$\overline{\psi}(x, y, t) = \left\{\overline{\varphi}(y)\ e^{-\alpha_i x}\right\} e^{j(\alpha_r x - \beta t)} \tag{16}$$

In this case, the value in the brackets is the spatial-dependent amplitude of a wave traveling in the x-direction with a frequency β and a wave number α_r. For amplification of disturbance, α_i must be negative ($\alpha_i < 0$).

Comparison with experiments has shown that the spatial amplification factor is more accurate than the temporal factor.

Thus, the relevant parameters for shear flow instability are:

α_i is the spatial amplification factor of disturbance, i.e. the rate of growth of disturbance in the streamwise direction.

α_r is the dimensionless wave number, $\alpha_r = 2\pi\theta/\lambda$, where θ is the momentum thickness and λ is the wavelength.

β is the dimensionless frequency, $\beta = 2\pi f\theta/U$

C is the phase speed, $C = \beta/\alpha_r$

In general, the velocity profile U(y) is known. For each frequency β, we solve Eq. (13) numerically to find α and ϕ which satisfy the boundary conditions. This gives α_I, the wavelength and the phase speed.

The results of the stability analysis are generally presented in the following form

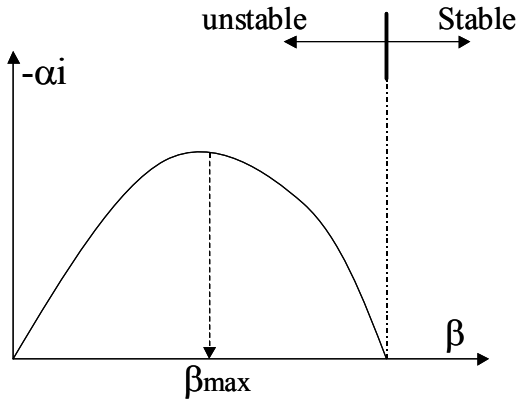

Schematic of the amplification rate as a function of dimensionless frequency

In addition to the above, the stability analysis yields the following general conclusions concerning shear flows

(i) Velocity profiles which possess a point of inflection are unstable. This means that free shear layers, jets, and wakes are inherently unstable.

(ii) The phase speed of the instability wave, i.e. the speed of disturbance propagation, is smaller than the maximum velocity of the mean flow.

3.4. Streamwise amplification and transition of a plane mixing layer

Figure (3.1) illustrates the main features of disturbance growth in a mixing layer. The linear hydrodynamic theory is applicable for the initial phase only and predicts the growth rate α_i. This initial region is referred to as the linear growth region although the disturbance grows exponentially by several orders of magnitude. Further downstream, the disturbance amplitude saturates and the instability wave rolls up into vortex-like structures at the fundamental frequency β_o. This is associated with the growth of the higher harmonic $2\beta_o$, and the sub-harmonic component $\beta_o/2$. The growth of the sub-harmonic component initiates the process of vortex pairing, where every two successive vortices join to form a single larger vortex. This results in halving the frequency of flow oscillation. These activities take place within the non linear and the transition regions. Further downstream, the higher harmonics grow stronger and the organized flow fluctuations break down into turbulence (Miksad, 1972).

A frequency spectrum of the velocity fluctuation is shown in the bottom of Fig. (3.1). It is seen that not only the fundamental component β_o is present, but the sub- and higher harmonics are also present. The strength of each of these components depends on both the streamwise and transverse location of velocity measurement. The amplification rates obtained from the linear stability theory for typical examples of shear flows are summarized in Fig. (3.2). In the next section, the theoretical predictions of growth rates for the hyperbolic tangent shear layer, Eq. (14), are compared with those obtained experimentally.

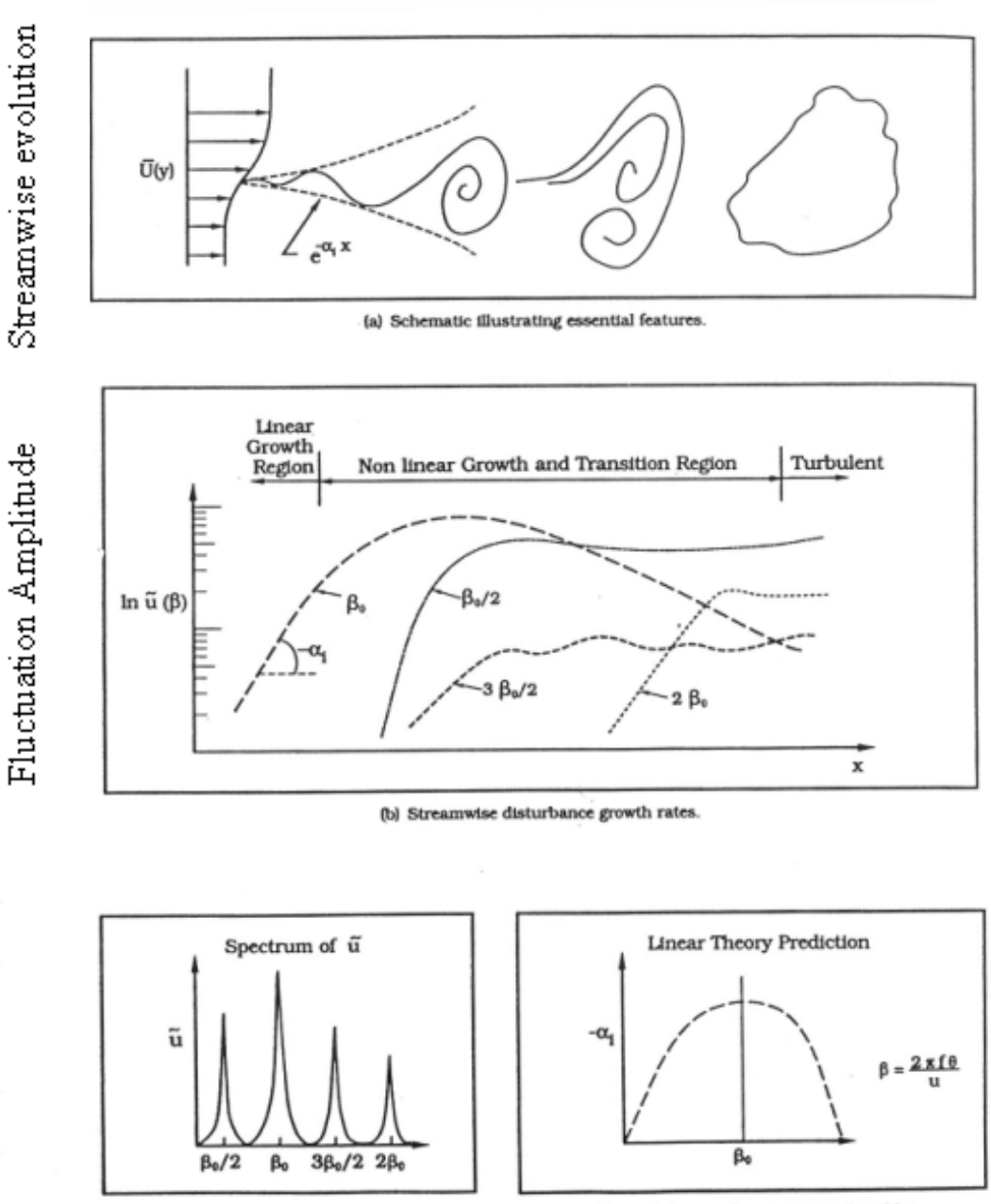

Figure 3.1. Schematic showing the main features of disturbance growth in a planar mixing layer (Lucas *el al.*, 1977).

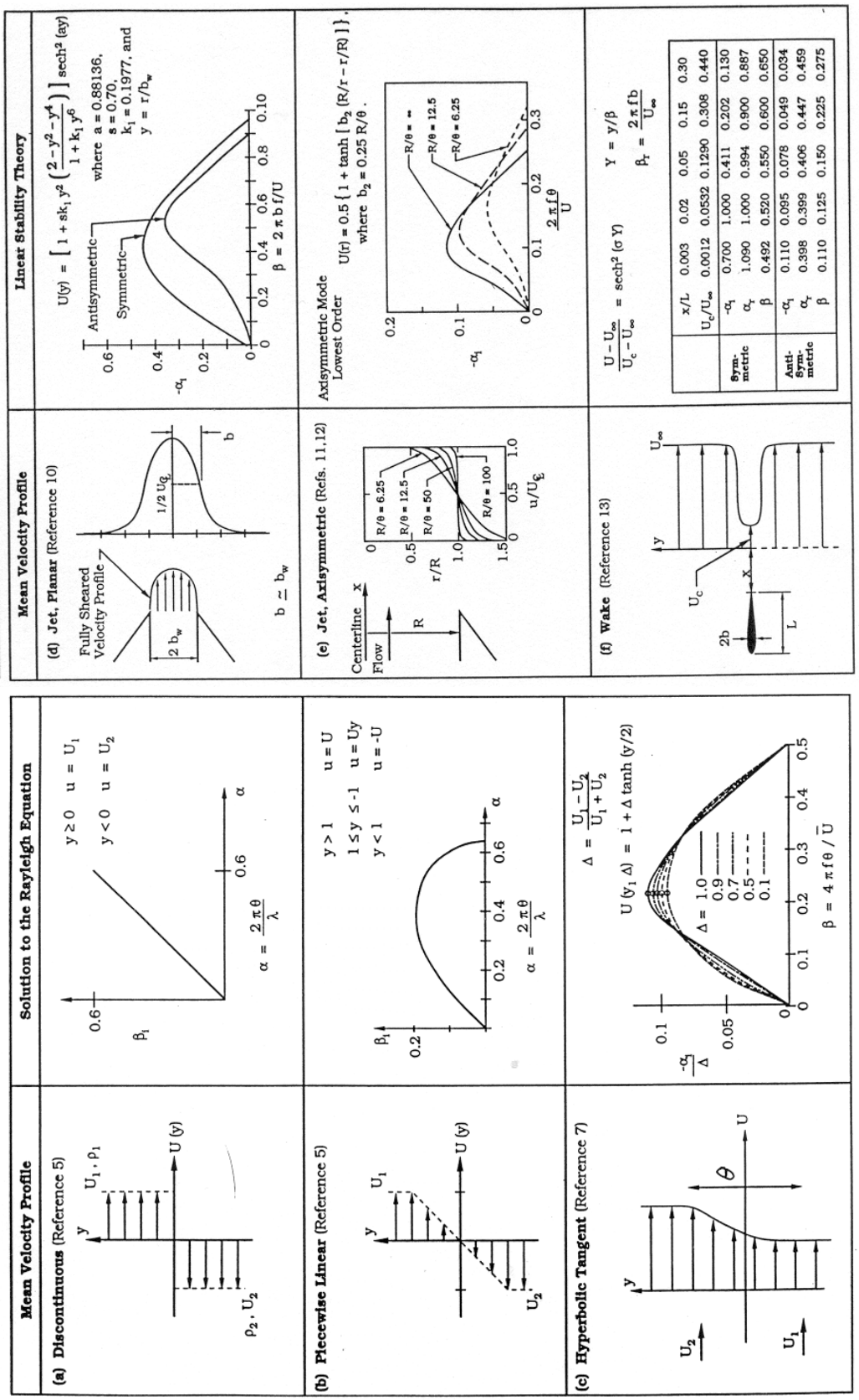

Figure 3.2. Solutions to the Rayleigh equation (i.e. prediction of the linear stability theory) for six mean velocity profiles (Lucas *el al.*, 1977).

3.5. Comparisons with experiments

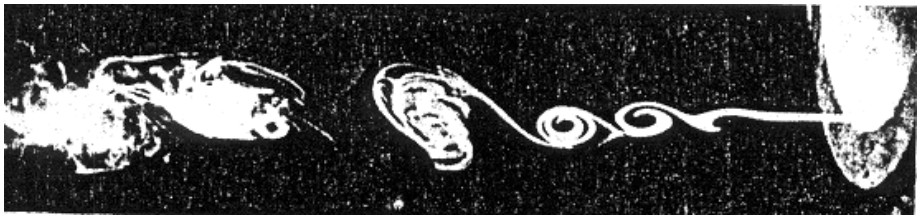

Flow visualization from Freymuth (1966)

Freymuth (1966) used loudspeakers to excite a round jet and investigated the amplification characteristics of the imposed disturbance along the shear layer which separates from the lip of the jet. Since it was possible to vary the frequency and the amplitude of excitation, the effect of these parameters on the instability of the shear layer was studied in some details. The following figure shows a smoke visualization photograph of the jet shear layer development (Freymuth (1966)).

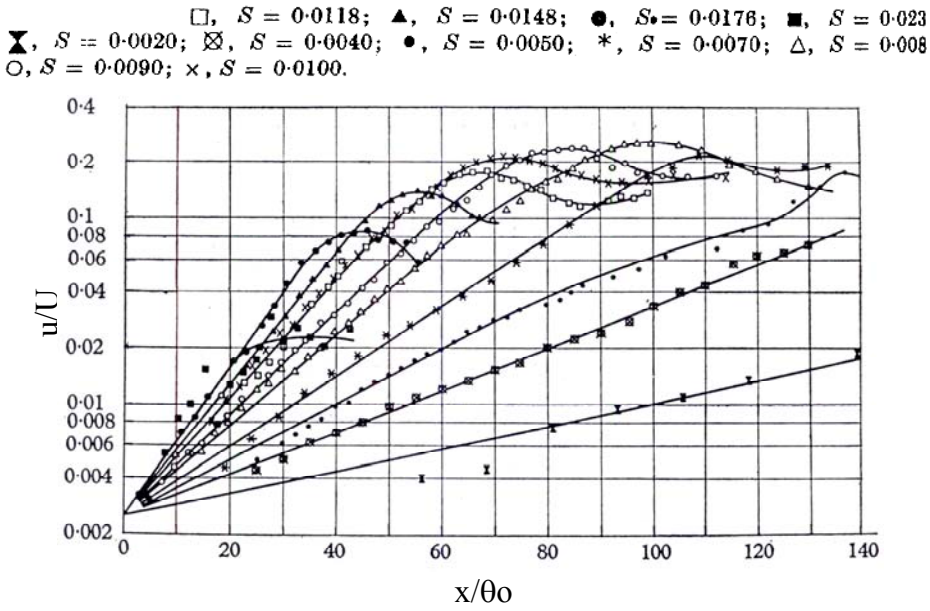

Figure 3.3. Dependance of the growth of velocity fluctuation on the Strouhal number.

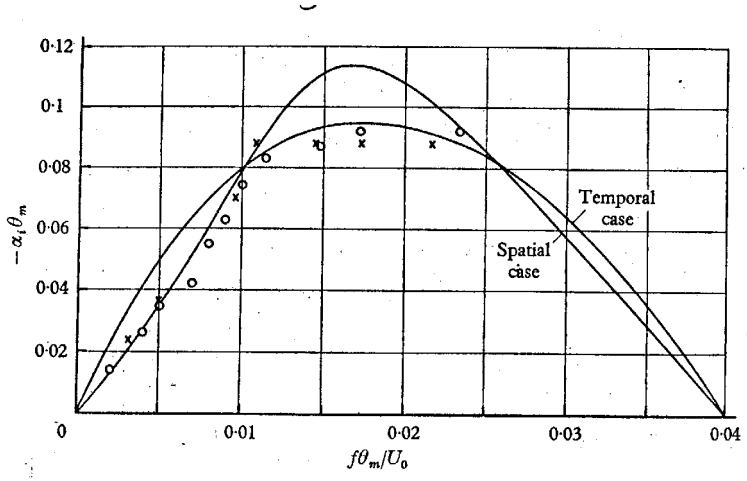

Figure 3.4. Growth rate versus Strouhal number. o: axisymmetric nozzle: x: plane nozzle (Freymuth, 1966).

By measuring the amplitude of the velocity fluctuations as a function of streamwise location, Freymuth (Fig. (3.3)) showed that the initial rate of disturbance growth is indeed exponential as the linear theory predicts. Interestingly, the disturbance which receives maximum amplification, for S = $f\theta/U = 0.0176$, saturates at about 8% of the mean velocity, U, whereas disturbances receiving lower amplifications grow to as much as 20% of the mean velocity. This figure also shows the nature of the shear layer instability; it acts as an amplifier whose gain and nonlinear amplitude saturation are frequency dependent. Figure (3.4) compares the measured amplification rates, which are the slopes of the lines shown in Fig. (3.3), with the linear theory. The agreement is seen to be very good.

4. Oscillations of Impinging Shear Flows *(The Fluid-Dynamic Mechanism)*

4.1. Effect of impingment

As stated earlier, the impingement of separated shear flows on solid objects generates a feedback mechanism, which sustains oscillations at *selected* frequencies from within that band of frequencies at which the flow is unstable. The effect of impingement is illustrated in Figures (4.1 & 4.2). The top photo in Fig. (4.1) shows the flow structure of a mixing layer between two streams impinging upon an edge, whereas the second photo was taken at the same flow conditions of the mixing layer but without the impingement edge. It is clear that the flow is much more organized and two-dimensional when the impingement edge is present. The bottom photo shows a large degree of streamwise vorticity, which rapidly destroys the two dimensionality of the flow.

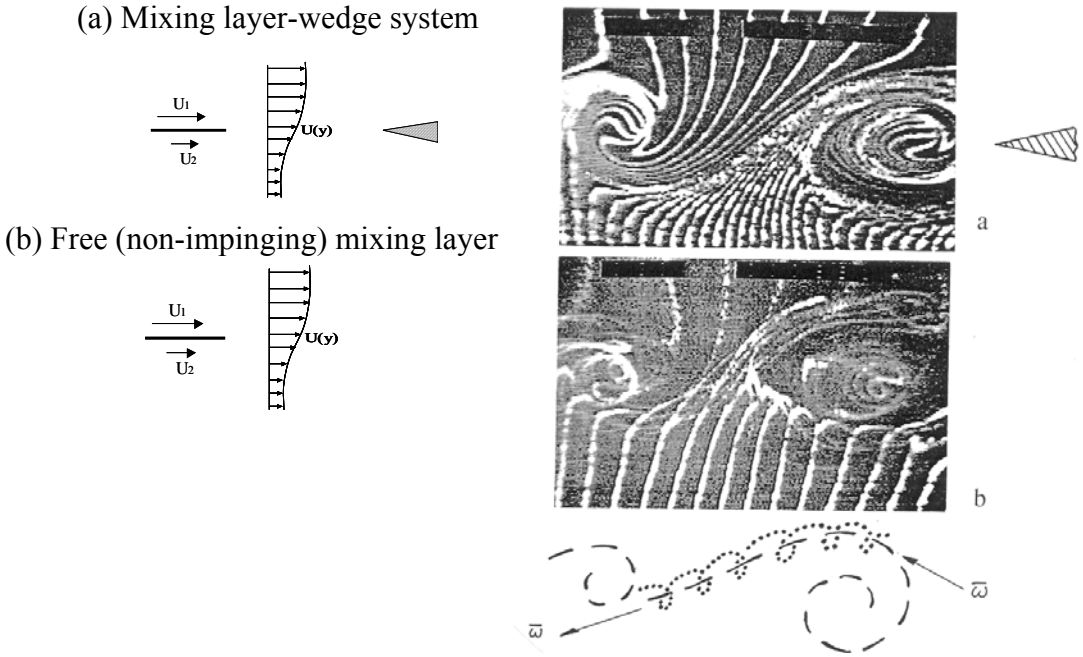

Figure 4.1. Hydrogen bubble visualization of a mixing layer (a) with impingement wedge, $L/\theta_0 = 79$; (b) without impingement wedge, $L/\theta_0 = \infty$, L is the impingement length, and θ_0 is momentum thickness at separation (Ziada & Rockwell, 1982).

Measurements of the velocity fluctuations, with and without impingement, of the same mixing layer discussed above are shown in Fig. (4.2). The flow impingement is seen to increase the velocity fluctuation at separation by at least an order of magnitude. This, together with the enhancement of the flow structure as illustrated in Fig. (4.1), results in a substantial increase in the saturation amplitude of the velocity fluctuation and therefore the fluctuating energy of the flow becomes much stronger when the impingement edge is added. Thus, the upstream feedback, which is generated from flow impingement, is seen to increase the amplitude of flow oscillations and to

preserve the two dimensionality of the flow. These are the basic ingredients which contribute to intense noise generation and excessive dynamic loading by the flow on neighbouring structures.

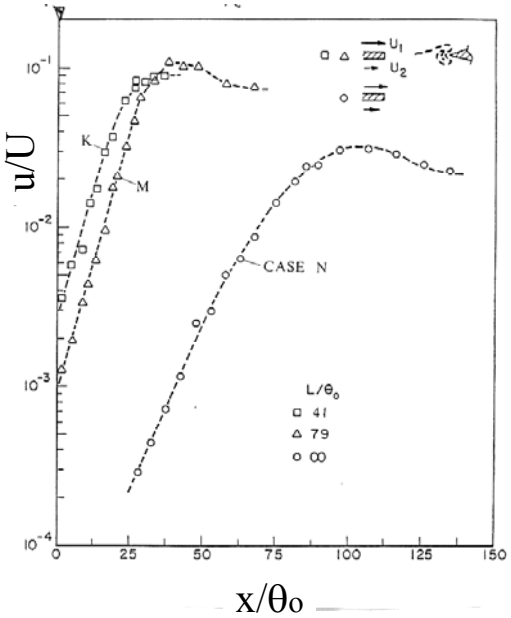

Figure 4.2. Effect of impingement on velocity fluctuation (u) along a mixing layer impinging upon an edge. Cases K& M with edge; Case N without edge. (Ziada & Rockwell, 1982).

4.2. The fluid-dynamic mechanism

As described by Naudascher and Rockwell (1994), the increase in the initial velocity fluctuation near the separation edge is due to the upstream feedback of pressure perturbations resulting from the downstream impingement of the vortex-like structures on the wedge. This upstream feedback is referred to in the literature as the fluid-dynamic feedback mechanism. It does not require any resonance effects to sustain the flow oscillation. This mechanism has been observed for a spectrum of configurations such as the jet-edge (Fig. (4.3)), jet-wall, jet-slot or hole and many others as illustrated in Fig. (4.4). All these flow configuration may exhibit strong oscillations excited by the fluid-dynamic mechanism whose basic events are illustrated in Fig. (4.3).

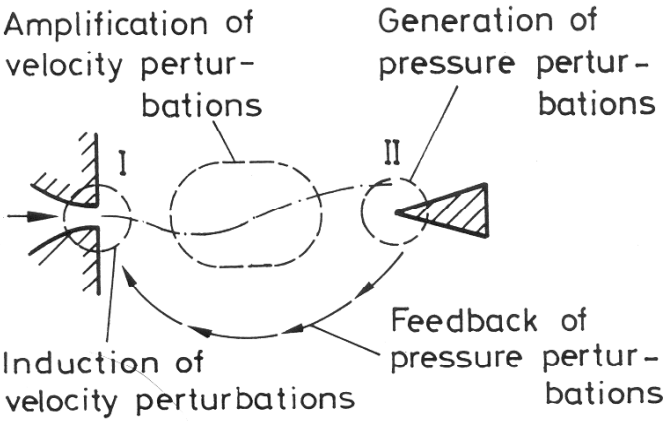

Figure 4.3. Fluid-dynamic feedback mechanism resulting from flow impingement (Naudascher and Rockwell, 1994).

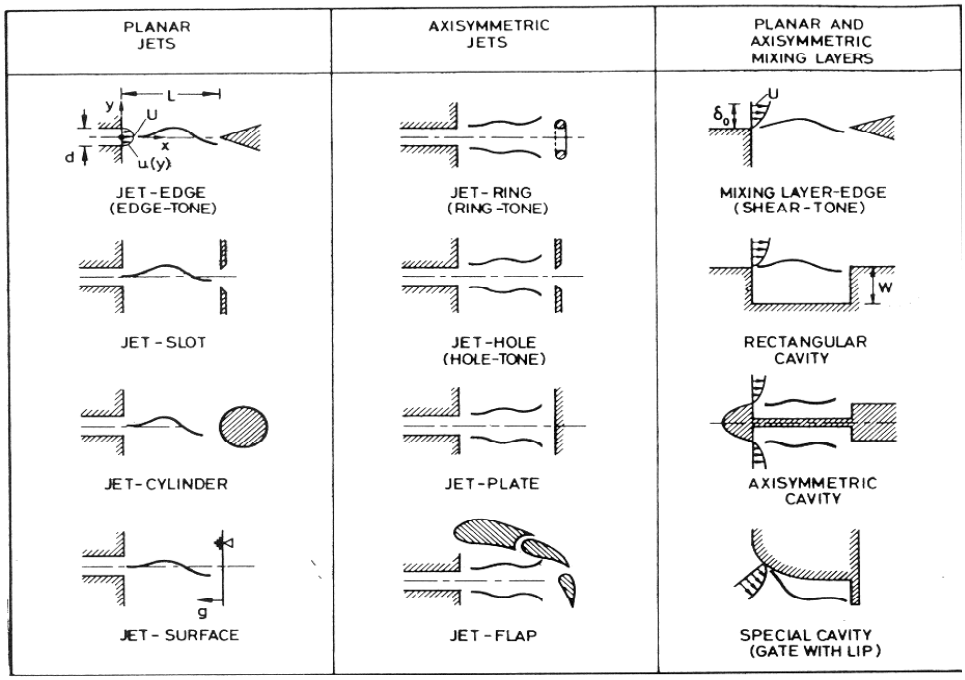

Figure 4.4. Basic configurations of shear layers and impingement-edge geometries that produce self-sustained oscillations excited by the fluid-dynamic feedback mechanism (from Naudascher and Rockwell, 1994).

At low Mach number flows, the impingement distance L is normally much smaller than the acoustic wavelength λ_a ($L/\lambda_a << 1$). This means that the flow separation location is within the non-propagating region of the impingement edge and therefore, the disturbances generated by flow impingement at the edge are instantaneously felt upstream at the location of flow separation. In other words, the upstream effect is purely hydrodynamic at low Mach number. At high speed flows, the acoustic wavelength may be comparable with the impingement length. In this case, one should take into account the time delay required by the disturbance to travel upstream from impingement edge to flow separation.

4.3. Examples of impinging shear flows

Oscillations of impinging shear flows occur at selected frequencies. This is because these oscillations have to satisfy a phase condition between flow activities near the separation and the impingement locations. When this condition is satisfied, the upstream feedback produces velocity fluctuation at separation, which is in phase with the shear layer oscillation. Applying this phase condition results in an approximate formula to predict the frequency of oscillations, f, which is normally given in terms of the Strouhal number, S_L, based on the impingement length, L:

$$S_L \equiv f\,L\,/V = (n + \varepsilon)\,C/V, \qquad n = 1, 2, 3, \ldots \tag{17}$$

where V is the flow velocity, C is the phase speed of the instability wave and ε is a constant (ε = 0 to 0.5). In general, ε and C/V depend on the particular system configuration and flow conditions. The integer n in Eq. (17) is the mode (or the stage) number. Thus, impinging shear flow oscillations occur at several modes, n, which are separated by frequency jumps. For example, as the impingement length, or the flow velocity, is increased, the oscillation frequency will change gradually until a critical value at which a frequency jump occurs. This jump marks the switching of oscillation to another mode. The mode number, n, represents the number of wavelengths (or vortices) between the separation and impingement locations.

Figure (4.5) shows plots of Strouhal number (fL/V) of the dominant oscillation for three typical examples of impinging shear flows: jet-edge, cavity, and shear layer-edge. All three cases show remarkable similarities in their frequency behavior as a function of the impingement length. Note the occurrence of frequency jumps between different modes (or stages of operation). For further details of this class of oscillations, the reader is referred to Rockwell & Naudascher (1978, 1979).

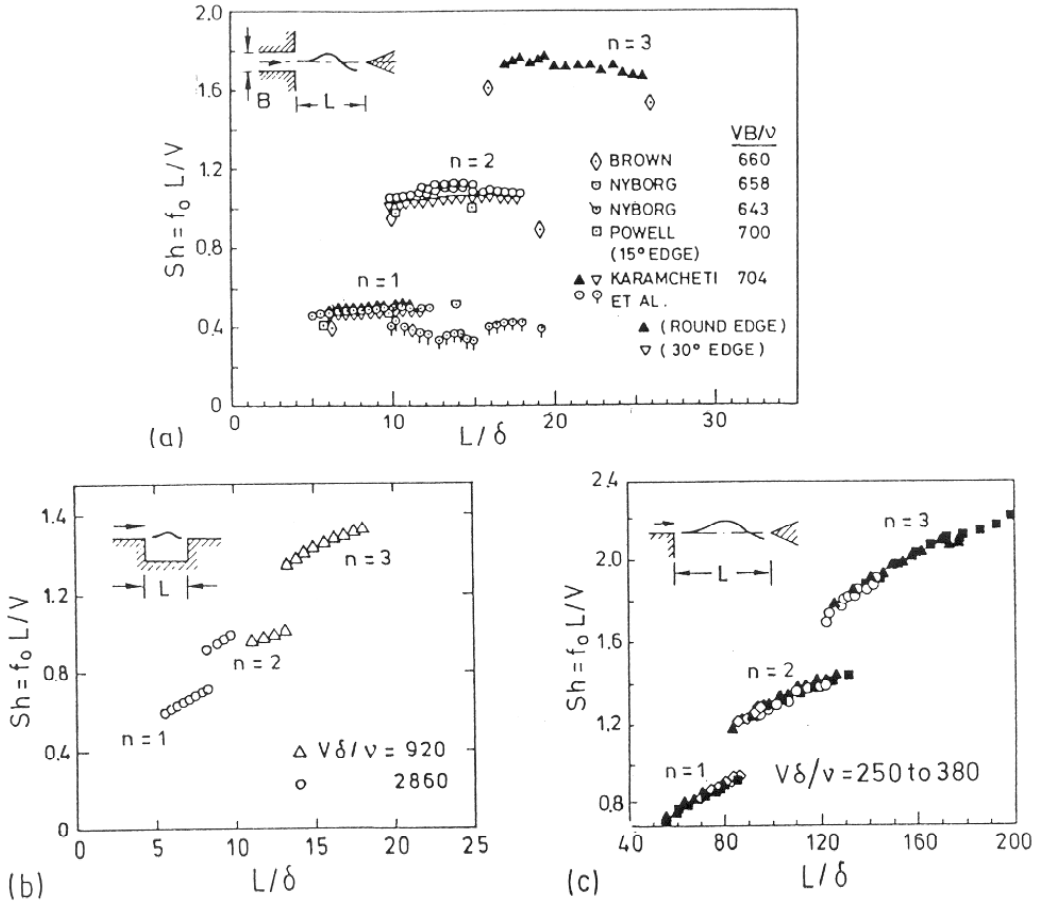

Figure 4.5. Strouhal numbers, fL/V, for (a) jet-edge oscillations; (b) cavity oscillations; and (c) mixing layer-edge oscillations, δ is the boundary layer thickness at separation (from Naudascher & Rockwell, 1994).

In the top photo, with upstream feedback effect, the velocity fluctuation at the jet exit is stronger and therefore the jet develops very rapidly and the transition to small-scale turbulence takes place after three shock cells only. Note that the jet-spread rate is remarkably steep.

When the upstream feedback is prevented, the bottom photo shows a much slower jet development, a smaller angle of jet spread, and five shock cells before the break down into turbulence. This is because the velocity fluctuation at the jet exit was reduced when the upstream effect was prevented by means of the reflectors. Thus, the upstream effect is always present, but it is weaker for non-impinging flows.

4.4. Feedback control of impinging shear flow oscillations

Since the most important event of the excitation mechanism is the upstream feedback, eliminating this feedback would break the cycle of events of the excitation mechanism and thereby suppresses the self-sustained oscillations. Ziada (1995) developed an active control technique to

counteract the upstream feedback. The basic idea of this technique is illustrated in Fig. (4.6), which shows a block diagram of the excitation mechanism, together with the *active control feedback*, which is added to counteract the *fluid-dynamic feedback*. In the case of an impinging planar jet for example, Fig. (4.7), this can be achieved by using loudspeakers which are focused on the jet exit only. The loudspeakers can be activated by the signal of a transducer sensing the jet oscillations, such as a microphone. This reference signal must be phase shifted and amplified optimally before it is used to activate the speakers. Figure (4.7) shows a simple controller consisting of a filter, a phase shifter and an amplifier. A digital controller with adaptive digital filter and a recursive root-mean-square algorithm was also used in order to be able to impose the proper phase and gain for each frequency within the frequency range of interest. The effect of feedback control using a digital controller on the jet-edge and jet slot oscillations is illustrated in the following.

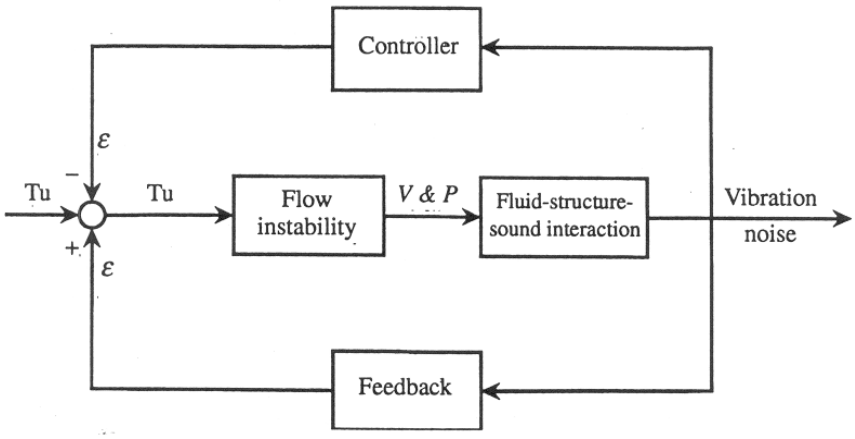

Figure 4.6. Block diagram presentation of the feedback mechanism causing self-excited oscillations and the basic idea used to suppress this mechanism by active means. Tu is the broadband flow turbulence, V & P are the velocity and pressure fluctuations, and ε is the upstream feedback (Ziada, 1995).

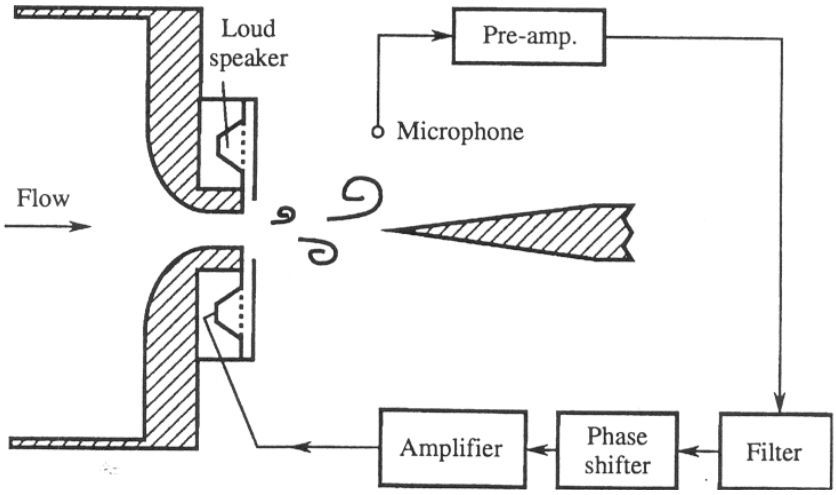

Figure 4.7. Schematic diagram of the test facility showing a two dimensional nozzle, a wedge (or edge), loudspeakers, and a flow diagram of the control circuit (Ziada, 1995).

Noise spectra of the jet-edge oscillations with and without control are shown in Fig. (4.8) for three values of Reynolds number. It is seen that the feedback control technique eliminated the system oscillations entirely, without destabilizing higher order modes. A reduction of about 30 dB

in the narrow band peak was achieved at all three Reynolds numbers. Similar reductions were also achieved in the case of the jet-slot oscillator (Ziada, 1995). Flow visualization photos of both the jet-edge and the jet-slot with and without control are shown in Fig. (4.9). In both cases, it is seen that the lateral oscillations of the jet and the organized vortical structures are totally eliminated by the developed control method.

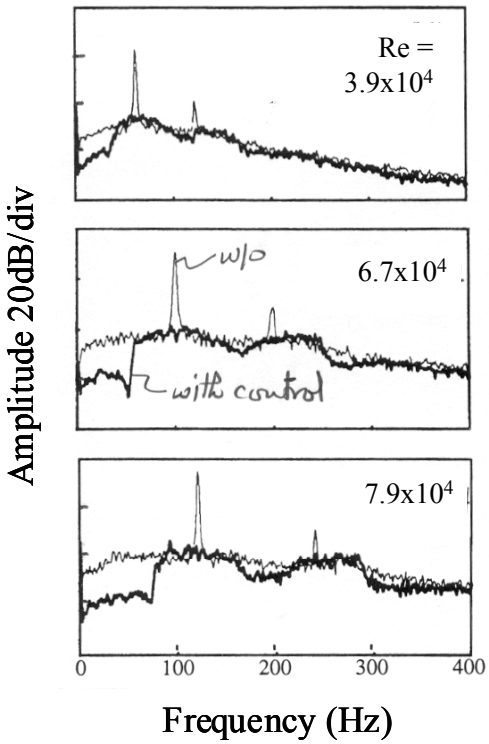

Figure 4.8. Effect of the adaptive digital controller on the noise spectra of the jet-edge oscillator illustrated for several Reynolds numbers. Thin line: without control; thick line: with control (adapted from Ziada, 1995).

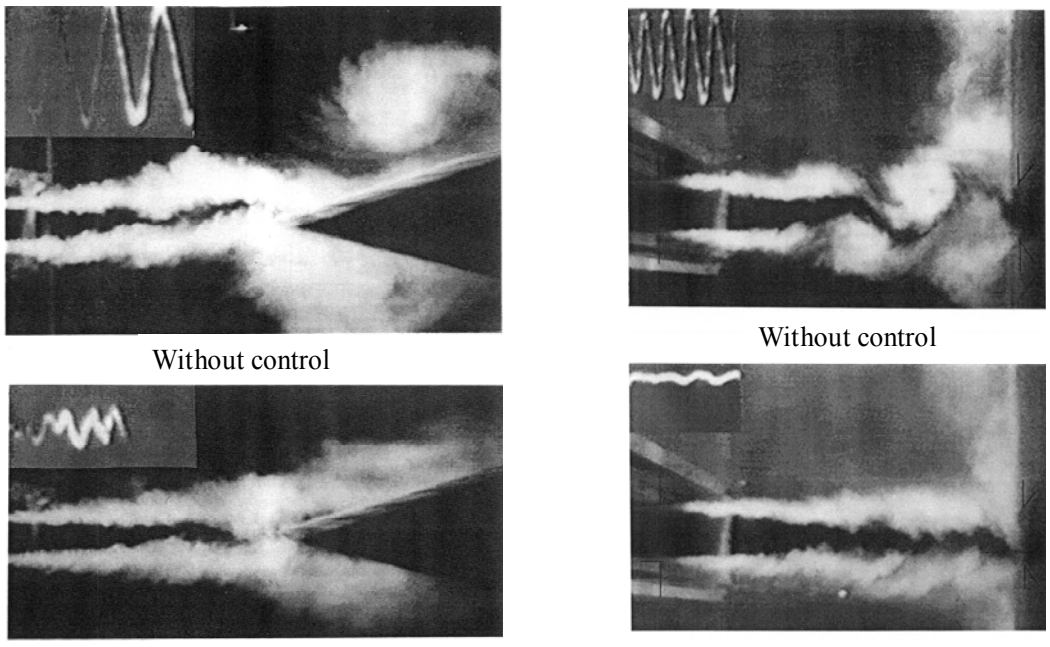

Without control

Without control

With control

With control

Figure 4.9. Flow visualization photos of the jet-edge (left) and the jet-slot (right) with and without control. The signal at the top left of each photo shows the microphone signal (Ziada, 1995).

The developed control technique has several advantages. First, the energy required to activate the control system is substantially reduced because the loudspeakers are focused on a small portion of the whole flow field. Secondly, since the jet exit is the most sensitive location and the velocity fluctuation is smallest there, the required power to cancel the flow feedback is minimized. Thirdly, in many practical applications, such as combustion oscillations (Ziada & Graf, 1998), the secondary sources cannot be installed to act directly on the flow field because of hazardous conditions. Connecting the secondary sources to the location of flow separation provides an alternative approach in such cases. Finally, since the control circuit is activated by the system response, the amount of power needed to suppress the oscillation continuously drops sharply after an initial short period. The loudspeakers therefore do not need to be as powerful as in the case of active noise cancellation.

5. Flow-Excited Acoustic Resonance

Flow-excited acoustic resonances are often encountered in many engineering applications involving internal or external flows. The acoustic pressure associated with such resonances can cause severe noise problems and, in some cases, endanger the structural integrity of the installation. Flow-excited acoustic resonance can occur in piping systems conveying gases or liquids, flow control devices, turbomachines, boilers, heat exchangers, cavities in fast moving vehicles, and many other applications. In many of these examples, the resonance is excited by an unstable separated flow, such as a shear layer, a jet or a bluff body wake. As mentioned earlier, Rockwell and Naudascher (1979) classified this excitation mechanism as *fluid-resonant* in contrast to the already discussed *fluid-dynamic* mechanism, which generates self-sustained oscillations of impinging shear flows in the absence of resonance effects. In the *fluid-resonant mechanism,* the resonant sound field provides the upstream feedback and excites the shear flow at its separation location and thereby sustains the oscillation. Although the fluid-dynamic mechanism by itself can generate strong flow oscillations, its coupling with an acoustic mode drastically increases the oscillation amplitude. This coupling, together with some of its consequences, is discussed in the next section by considering the interaction mechanism between a jet-slot oscillator and a deep cavity resonator.

5.1. An example of impinging shear flow coupling with an acoustic resonator

Figure (5.1) shows a planar jet impinging on a slot, which constitutes a jet-slot oscillator excited by the fluid-dynamic mechanism. However, in this case, an acoustic resonator is added which consists of two well-tuned deep cavities. The acoustic pressure distribution of the first acoustic mode of the deep cavities is also shown. This mode consists of a half-wavelength acoustic wave with a pressure node at the jet centerline. Attention is now focused on the changes which may occur in the nature of jet oscillation when the acoustic resonance is developed, or attenuated, as the flow velocity is increased. It will be shown that the occurrence of resonance may be associated with a fundamental change in the mode of jet instability, and in some cases, associated also with a jump in the frequency of oscillation.

The frequency, f, and the dimensionless amplitude, P, of the dominant component of pressure oscillations are plotted in Fig. (5.2) as functions of the flow velocity at the nozzle exit, V. The pressure amplitude is normalized by the jet dynamic head, i.e.

$$P = P_{rms} / (\tfrac{1}{2} \rho V^2) \tag{18}$$

Here P_{rms} is the root-mean-square amplitude and ρ is the density. The results shown in Fig. (5.2) were measured by means of Microphone 1 (see Fig. (5.1)), and have been found to be almost identical to those obtained by Microphone 2.

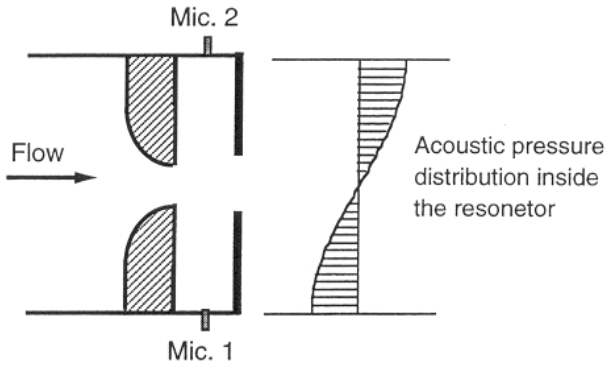

Figure 5.1. Schematic of the experimental set-up to investigate the interaction mechanism between a jet-slot oscillator (with a fluid-dynamic feedback) and an acoustic resonator consisting of two well-tuned deep cavities (Ziada, 2001).

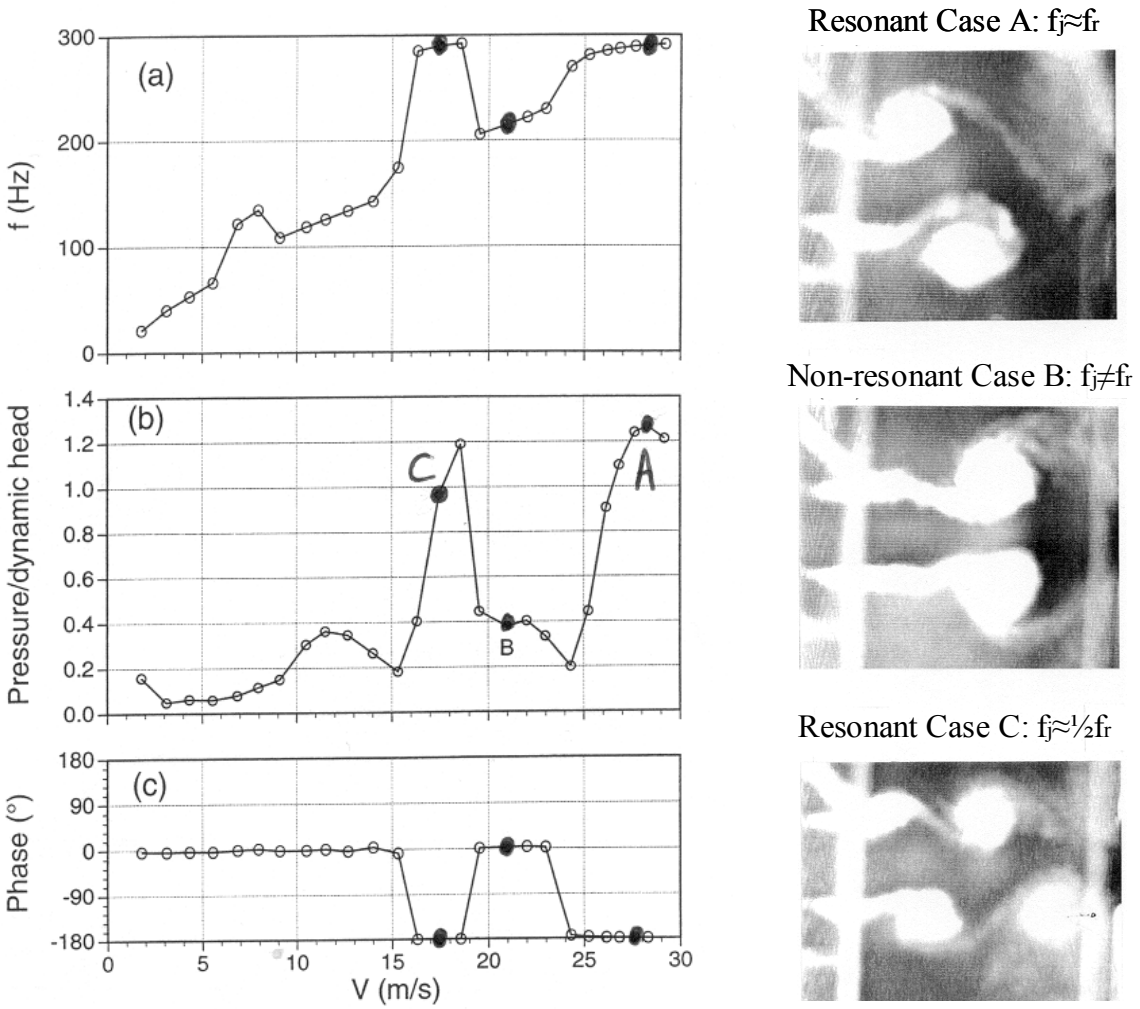

Figure 5.2. Response of a jet-slot oscillator combined with a cavity resonator: (a) frequency of oscillation; (b) normalized acoustic pressure; (c) phase between pulsations in cavities; right-hand side: visualization of non-resonant case B and resonant cases A & C (Ziada, 2001).

The phase angle between Microphones 1 & 2 is given in Fig. (5.2(c)). Resonance of the acoustic standing waves along the cavity depth, Fig. (5.1), is seen to occur over two ranges of flow velocity, between V = 16-19 m/s and at V > 24 m/s. Within these ranges, the oscillation frequency (≈ 292 Hz) agrees well with that calculated from the formula:

$$f = c / 2H \tag{19}$$

Here c is the sound speed and H is the distance between the cavities closed ends (590 mm).

Outside the resonance ranges, where the flow oscillations resemble the natural oscillation mode of the jet-slot oscillator (the fluid-dynamic mechanism), the frequency increases smoothly with the flow velocity and the pressure oscillations in the two cavities are in phase. This suggests that the jet oscillates symmetrically when the acoustic resonance is not excited. This is illustrated to be indeed the case by the flow visualisation photograph corresponding to Case B in Fig. (5.2). At the onset of resonance, the pressure amplitude increases sharply with flow velocity and the pressure oscillations in the cavities become out of phase with each other as illustrated in Fig. (5.2(c)). Thus, the jet oscillation pattern switches to an anti-symmetric mode when the resonance is excited, as can be seen from the flow visualisation photos corresponding to the resonant cases A & C. At the onset of the first resonance range (V ≈ 16 m/s), the oscillation frequency is approximately doubled. This indicates that when the resonance sets in, the jet oscillation switches not only from a symmetrical to an anti-symmetrical mode, but also to a higher mode of the jet oscillation, whereby the number of the formed vortices along the cavity mouth is increased. The excitation of acoustic resonance by higher order modes of the shear layer has been reported for several other cases such as a pipeline with two baffles (e.g. Hourigan et al., 1990) and a pipe with closed side branches (e.g. Graf & Ziada, 1992; and Ziada, 1993).

As indicated in Fig. (5.2), the oscillation amplitude is increased substantially when the resonance is excited. This enhancement is due to the fluid-resonant mechanism, which is described in the following section.

5.2. The fluid-resonant mechanism

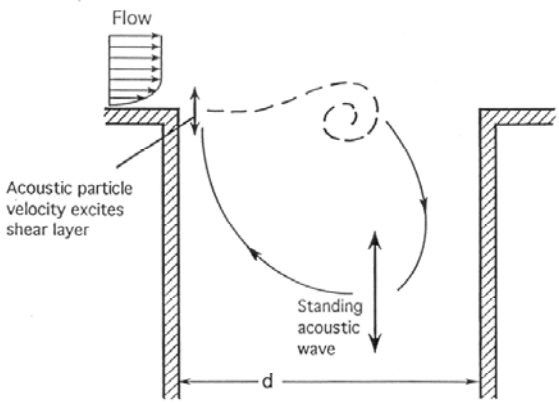

Figure 5.3. Main events of fluid-resonant mechanism for deep cavity acoustic resonance excited by grazing flow.

The mechanism by which impinging flows excite acoustic resonances is illustrated in Fig. (5.3). At the upstream separation edge, the resonant sound field induces velocity perturbations in the shear layer. Blevins (1985), for example, has shown that high intensity sound waves can shift the frequency of vortex shedding from that of natural shedding. The velocity perturbations, which are

induced at the upstream separation edge, extract energy from the mean flow and grow exponentially in the downstream direction into vortex-like structures. Further downstream, near impingement, the phase of the sound cycle becomes favourable and the vortex structures generate acoustic energy which enhances the resonant sound field.

Substantial progress in understanding and modelling this excitation mechanism has been achieved since Howe (1975, 1980) formulated his acoustic analogy in which vorticity is identified as a source of sound. He showed that the instantaneous acoustic power, $\mathcal{P}$, generated by vorticity, $\boldsymbol{\omega}$, convecting within a sound field is given by

$$\mathcal{P} = -\rho \int \boldsymbol{\omega} \cdot (\mathbf{v} \times \mathbf{u})\, d\forall \qquad (20)$$

where ρ is the fluid density, $\mathbf{v}$ is the fluid velocity, $\mathbf{u}$ the particle velocity of the sound field and $\forall$ is the volume containing the vorticity field. Whether vorticity acts as acoustic source or sink (i.e. whether acoustic energy is generated or absorbed) depends on the triple product $\boldsymbol{\omega}$. ($\mathbf{v}$ x $\mathbf{u}$). Resonances are self-sustained if the integral of the sound power over an acoustic cycle is positive, and this implies that a favourable timing of vorticity convection with respect to the sound cycle must be maintained. Stoneman et al. (1988), Bruggeman (1987), Hourigan et al. (1990) and others have used Howe's theory to explain several features of flow-excited acoustic resonances, especially for the case of impinging shear flows. For example, the feature that resonances always occur within a certain range of Strouhal numbers is found to be related to the fulfilment of the above-mentioned phase condition over this range of Strouhal numbers, and therefore a net positive sound energy is produced over a complete cycle.

6. Acoustic Resonance of Closed Side Branches

6.1. Introduction

As an example of the fluid-resonant mechanism, the phenomenon of acoustic resonance in closed side-branches is considered in some detail. This particular example is rather important because closed side-branches are often encountered in gas and oil pipelines, steam, gas and water piping in power plants and chemical industry, exhaust gases conduits of boilers and engines, and many other industrial applications. The flow over the mouth of the branch can excite strong acoustic resonance of the side branch (see Fig. (5.3)). A pipe system is very much more liable to acoustic resonances if it has multiple closed branches in close proximity. An example of safety valves attached to a fresh steam pipe in a power plant is shown in Fig. (6.1). This pipe arrangement is a combination of co-axial and tandem branch arrangements as shown in Fig. (6.2). These arrangements can generate very strong acoustic resonance and dangerous pipe vibration (Ziada & Buehlmann, 1992)). Another example of multiple closed side-branches, which is often encountered in practical applications, is the piping system used in power plants to bypass the turbine. The branch pipes of this system are usually closed by means of the bypass control valves during normal operation of power plants. This section focuses on several aspects related to the phenomenon of acoustic resonance of single and multiple side-branches, prediction of the critical flow velocity for the onset of resonance, estimation of the pulsation amplitude, and possible counter-measures to reduce the pulsation amplitude. For further details, the reader is referred to a detailed study reported by Ziada (1993).

6.2. Characteristics of acoustic resonance

Figure (6.2) shows four typical arrangements of side-branches together with schematic presentations of their lowest acoustic resonance modes. The patterns of the acoustic flux associated

with these modes are shown in Fig. (6.3), which considers the cases for which both the distance between the branches, ℓ, and the main pipe diameter, D, are much smaller than the wavelength of the acoustic modes.

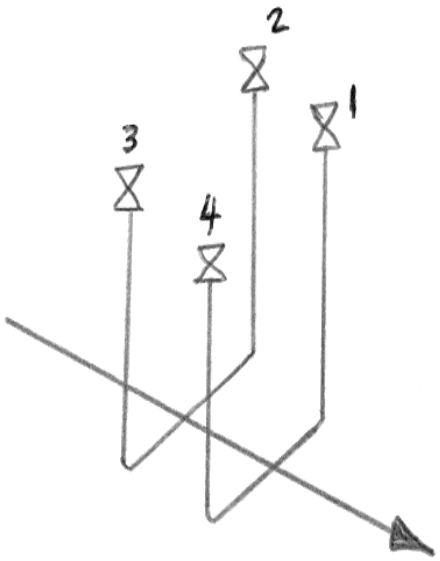

Figure 6.1. An example of four relief valves attached to a fresh steam line in a power plant.

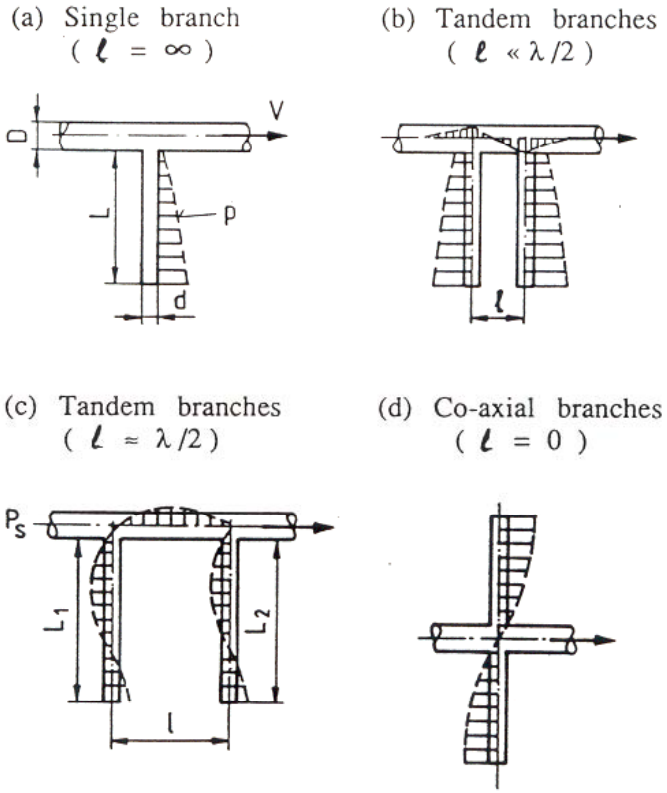

Figure 6.2. Typical geometries of side-branches and simplified patterns of acoustic pressure distributions of the resonance modes (Ziada & Buehlmann, 1992).

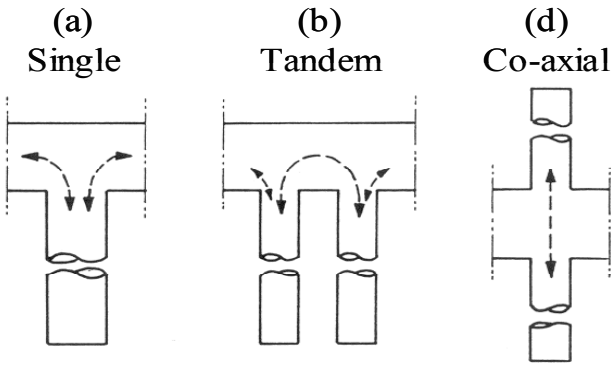

Figure 6.3. Single, tandem and co-axial closed side-branches showing the acoustic flux of the resonant acoustic mode (Ziada 1994).

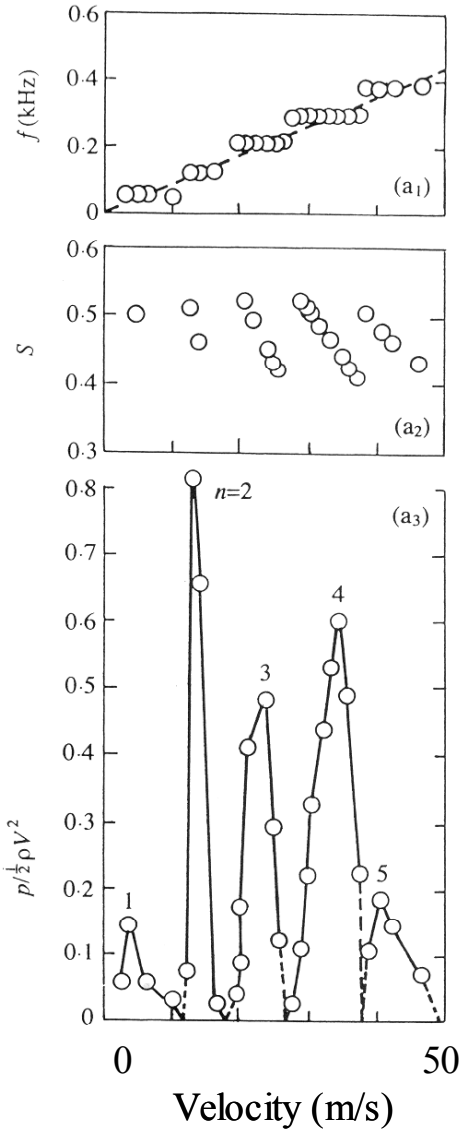

Figure 6.4. Acoustic response of two tandem branches as function of the flow velocity showing the frequency, the Strouhal number and the amplitude of various acoustic modes of the branches (Ziada & Buehlmann, 1992).

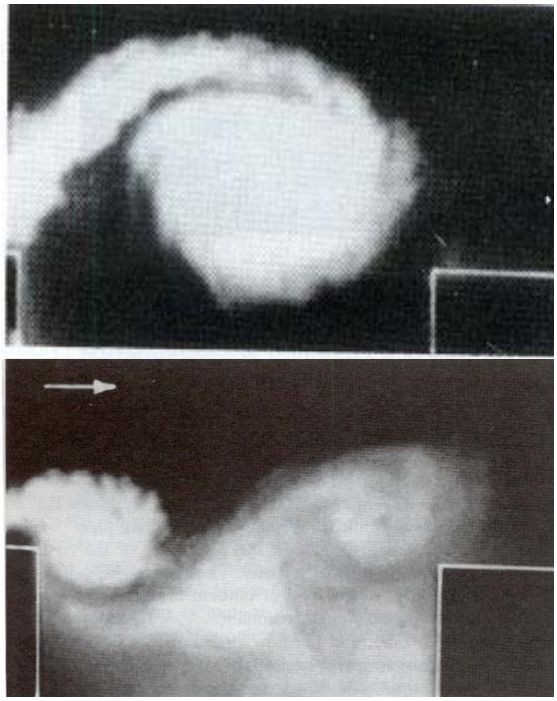

Figure 6.5: Flow visualization of the shear layer at the mouth of the branch whilst the resonance is excited. Top: first mode of the shear layer (n = 1); bottom: second mode (n = 2). Adapted from Ziada (1994).

In the single branch case, Fig. (6.3(a)), the pulsation amplitude in the branch is strongly influenced by the acoustic radiation into the main pipe, and consequently by the friction and heat losses in the main pipe as well as by the radiation losses at the main pipe terminations. For example, increasing the diameter of the branch, *d*, with respect to that of the main pipe, *D*, which increases the acoustic radiation into the main pipe, is associated with a rapid reduction in the pulsation amplitude at resonance.

In the case of two branches, Fig. (6.3(b & d)), which are well tuned (i.e. of equal length) and in close proximity, i.e. $\ell \ll \lambda$, the acoustic flux at the mouth of one branch is equal but opposite to that at the mouth of the other branch. In the case of the co-axial branches for example, Graf & Ziada (1992) found that only 2% of the branches acoustic power is radiated into the main pipe. The two branches therefore strongly couple and form a subsystem with negligible radiation losses into the main pipe. Thus, the pulsation amplitude in the case of two (or multiple) branches can be drastically higher than that in the case of a single branch. Ziada & Bühlmann (1992) and Ziada (1999) have shown that this is particularly the case for large values of *d/D*.

As an example, Fig. (6.4) shows the acoustic response of two tandem branches as a function of the flow velocity. It is seen that the resonance modes are excited consecutively, and during the resonance of each mode, the frequency remains constant, i.e. locked-in to the resonance frequency. During this process, the Strouhal number, S = fd/V, remains within the range of 0.4 to 0.5. As will be shown later, the Strouhal number at the onset of resonance is not constant, but is strongly dependant on the diameter ratio, d/D, and the approach flow conditions.

Figure (6.5) shows flow visualization pictures of the oscillation of the shear layer at the mouth of the branch whilst the resonance is excited. The resonance can be excited by the fundamental shear layer mode (top photo, n = 1) as well as by the higher modes (bottom photo, n = 2).

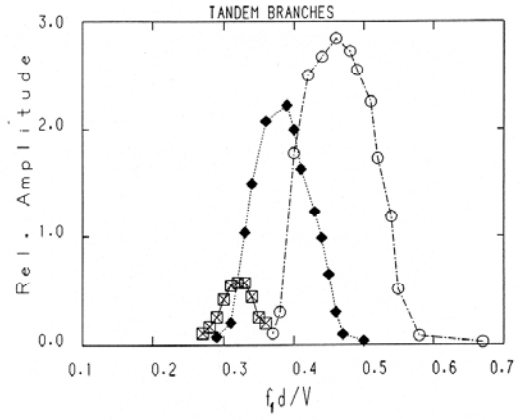

Figure 6.6: Effect of the diameter ratio on the critical Strouhal number at the onset of resonance and on the intensity of resonance for tandem side-branches. □, d/D = 0.135; ◆, 0.25; ○, 0.57 (Ziada & Shine 1999).

6.2.1. Effect of the diameter ratio

Figure (6.6) shows typical resonance curves of tandem branches with different diameter ratios. It is clear that the resonance range, and in particular *the onset of resonance*, S_o, shifts to a lower Strouhal number (i.e. to a higher velocity) when the diameter ratio, d/D, is decreased. The critical Strouhal number, S_o, is defined as:

$$S_o = f_1 \, d / V_o \tag{21}$$

Here f_1 is the lowest resonance frequency, d is the branch diameter, and V_o is flow velocity in the main pipe at the onset of resonance. The effect of d/D on S_o is seen to be quite strong and should be taken into account when evaluating the liability of a system to resonance.

The relation between S_o and d/D stems from the alteration of the convection velocity of the vortices forming at the branch mouth when *d/D* is varied. This is because the size of the formed vortices scales with the diameter of the side-branch (Ziada, 1994). Since the boundary layer thickness in the main pipe is *independent of the side-branch diameter*, a larger size vortex formed at the mouth of the branch-pipe will experience a higher mean velocity and will be swept faster along the branch mouth. The phase condition for the onset of oscillation, i.e. the favourable phasing between the vortex convection velocity and the acoustic oscillation, will therefore be achieved at a lower reduced velocity when the diameter of the side-branch (and consequently the vortex size) is larger.

6.2.2. Effect of upstream elbows

Resonances are initiated when the convection velocity of the shear layer vortices is increased to an appropriate value such that a net positive acoustic energy is generated over a complete cycle. Thus, when the mean velocity profile in the main pipe is not uniform, one would expect the onset of oscillation to be related to the "local" flow velocity at the mouth of the branch. In order to investigate this aspect, an elbow with a radius of 3D was installed upstream of the branch. The distance $\mathcal{L}$ between the elbow and the branch was varied from 1.8 to 10D. The effect of the upstream elbow was investigated for the cases of single, tandem and co-axial branches. As an example, the acoustic response of a single side-branch (d/D = 0.135) excited by a uniform flow ($\mathcal{L}$ /D = ∞) is compared in Fig. (6.7) with that excited by the (non-uniform) flow at the outlet of the elbow. The figure shows the results when the side-branch was installed first at the inner and then at

the outer side of the elbow. The relative amplitude ($P/_{1/2}\rho V^2$) and the Strouhal number are based on the average velocity calculated from the measured flow rate. The elbow is seen to affect the lock-in range and the amplitude of pulsation.

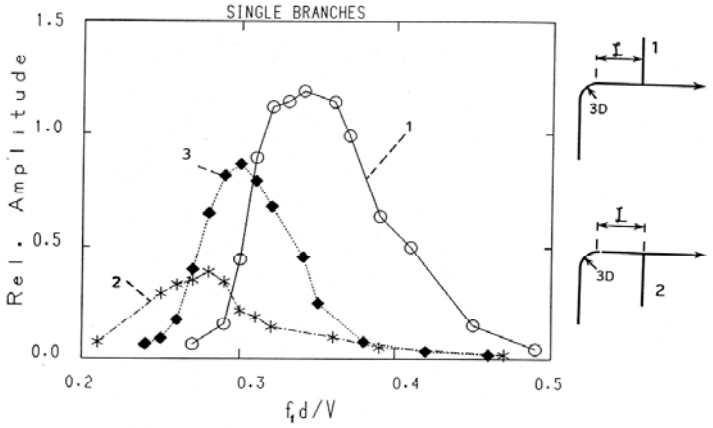

Figure 6.7. Effect of an upstream elbow on the acoustic response of a single branch. ○, branch at the outer side of the elbow; ∗, at the inner side; ◆, no elbow. d/D = 0.135, f_1 = 490 Hz, $\mathcal{L}$/D = 1.85, test pressure = 3 bar (Ziada & Shine 1999).

When the branch is at the outer side of the elbow, curve 1 in Fig. (6.7), the local velocity is higher than the average velocity. The resonance therefore starts at a lower flow rate, i.e. at a higher S_o (≈ 0.45). Moreover, the relative amplitude becomes higher than the case of uniform flow (curve 3 for which $S_o \approx 0.37$). This increase however is rather superficial because the relative amplitude is based on the average velocity, which is lower than the local velocity at the mouth of the branch, which excites the resonance. Conversely, when the branch is at the inner side of the elbow, curve 2 in Fig. (6.7), the onset of resonance is delayed, $S_o \approx 0.33$, i.e. it occurs at a higher flow rate, and the relative amplitude becomes (superficially) smaller.

The effect of the elbow on the critical Strouhal number is weakened when the distance $\mathcal{L}$/D between the elbow and the branch is increased. This feature is depicted in Fig. (6.8), which shows measurements of a single branch with d/D = 0.25 located at different distances from an upstream elbow. It is noteworthy that the effect of the elbow is still discernible also when it is located at 10D upstream of the side-branch.

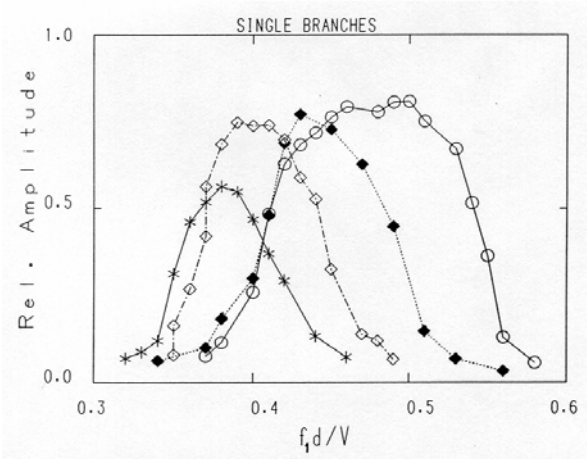

Figure 6.8. Pulsation amplitude verses Strouhal number for a single branch located at the outer side of, but at different distances ($\mathcal{L}$) downstream of an elbow. d/D = 0.25, f_1 = 326 Hz; ○, $\mathcal{L}$/D = 1.8; ◆ , 6.2; ◇ , 10; ∗ , ∞.

In the case of tandem branches also, the elbow promotes the onset of resonance and increases the relative amplitude of pulsation, whereas in the co-axial case, it has only a negligible effect. This difference seems to be due to the fact that the local flow velocities at the mouths of both branches are similar, and higher than the mean velocity, in the tandem case, but different in the coaxial case. Further details can be found in Ziada & Shine (1999).

6.3. Prediction of resonance

Assessment of the liability of a piping system to flow-excited acoustic resonance consists of two steps. First, the critical flow velocity for the onset of resonance is estimated. If this velocity is found to be within the operating range, the pulsation amplitude should be estimated to evaluate whether suitable counter-measures are needed.

6.3.1. Prediction of critical flow velocity

It has been shown that the main parameters that influence the Strouhal number at the onset of resonance (S_o) are the diameter ratio d/D and the distance from an upstream elbow (ℓ/D), if there is any. Although the radiation and viscous losses strongly influence the maximum amplitude at resonance and the width of the lock-in range, they have been found to have a negligible effect on S_o (Ziada & Shine, 1999). The Strouhal number data are therefore plotted as a function of the distance ℓ/D in Fig. (6.9), where the ratio d/D is taken as a parameter. It is seen that the value of S_o varies over a wide range ($0.35 < S_o < 0.62$). *Thus, there is not a single value of* S_o *which is applicable for all diameter ratios*. In fact, the author observed lower values of S_o in industrial applications with very small diameter ratios ($d/D < 0.1$).

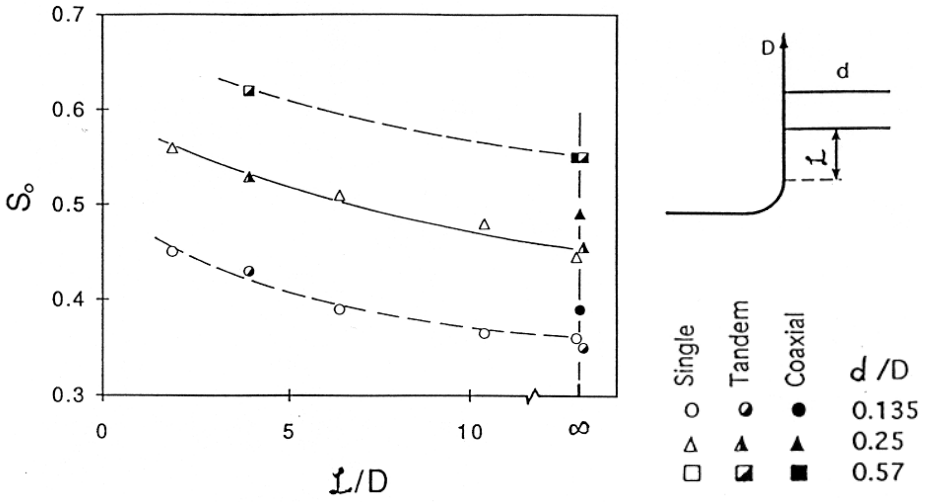

Figure 6.9. Design chart of critical Strouhal number at the onset of resonance adapted from Ziada & Shine (1999). For proper use see comments in the text.

The critical flow velocity (V_o) for the onset of resonance can be calculated from Eq. (21), where, S_o is the value obtained from Fig. (6.9). If the maximum flow velocity of the installation V_{max} is lower than V_o, resonance will not occur. Whenever V_o is found to be lower than V_{max}, design modifications should be adopted to make $V_{max} < V_o$. *This can be achieved by enlarging the branch diameter at the junction or by shortening the branch length to increase* f_l. If these simple modifications are not possible, or they do not result in a sufficient increase in V_o, the pulsation amplitude at resonance should be estimated as outlined by Bruggeman (1987) or Graf & Ziada

(1992). The estimation of the pulsation amplitude indicates whether it is necessary, or not, to implement additional counter-measures such as those described by Ziada (1993).

Several remarks should be made here regarding the use of the Strouhal number chart given in Fig. (6.9). First, when single or tandem branches are installed at the inner side of an upstream elbow, the critical Strouhal number is lower than that for $\mathcal{L}/D = \infty$, see Fig. (6.7). In such cases, the use of a value corresponding to $\mathcal{L}/D = \infty$ is recommended because it results in conservative designs. Secondly, since the effect of upstream elbows on the critical Strouhal number of co-axial branches is negligible, a value corresponding to $\mathcal{L}/D = \infty$ should be used for co-axial branches regardless of their position with respect to upstream elbows. Thirdly, it should be noted that Fig. (6.9) is developed from the test results of one elbow radius. However, since this radius is relatively small (3D), the present results would be conservative for many practical applications which may involve an elbow with radius larger than 3D. If the radius is smaller than 3D, the designer should consider an additional margin of safety.

The developed chart can be used also for side-branches with square or rectangular cross-sections. However, the diameter d in the Strouhal number formula must be replaced by the equivalent diameter proposed by Bruggeman (1987):

$$d_e = (4/\pi)\, H \tag{22}$$

where H is the width of the branch mouth in the flow direction.

When the corners of the branch mouth are rounded with a radius of curvature r, the critical flow velocity scales with (d + r) instead of d (Bruggeman (1987)). Figure (6.9) however, can still be used to estimate V_o by means of the formula:

$$V_o = f_1\, (d + r)/S_o \tag{23}$$

Finally, the value corresponding to d/D = 0.57 can be used for larger diameter ratios. This suggestion is based on the fact that the Strouhal numbers reported by Peters (1993) for d/D = 1 are similar to the present results for d/D = 0.57.

6.3.2. Estimation of resonance amplitude

When the side-branch is at resonance, the excitation mechanism becomes highly non-linear. In order to estimate the amplitude of pulsation, the shear layer instability and its interaction with the resonant sound field must be described by means of the non-linear theory. This rather complex approach does not seem suitable for industrial applications.

Graf & Ziada (1992) proposed a new approach to predict the pulsation amplitude at resonance. They modeled the integrated effect of the shear layer excitation by a complex source term, Q, and measured its amplitude and phase for a wide range of Strouhal number. Figure (6.10) shows the measured source term in a complex Q-plane. The Strouhal number and the pulsation amplitude, U, are taken as parameters. The pulsation amplitude U represents the ratio between the acoustic particle velocity at the branch mouth (u) and the mean velocity (U = u/V). Since the excitation mechanism is non-linear, the source term is a function of the pulsation level U.

The source term represents the ratio between the induced acoustic pressure difference across the shear layer ΔP and the acoustic particle velocity at the mouth of the branch. This ratio is normalized

by the dynamic head and the mean velocity. Thus, Q has the form of a dimensionless acoustic impedance:

$$Q = \Delta P / (\tfrac{1}{2}\rho V^2 U) \qquad (24)$$

In Fig. (6.11), the predicted amplitudes using the measured source term Q are compared with the experimental data for three cases of symmetric co-axial branches ($L_1 = L_2 = 0.61$, 1.105 & 1.585 meter). The agreement is seen to be very good.

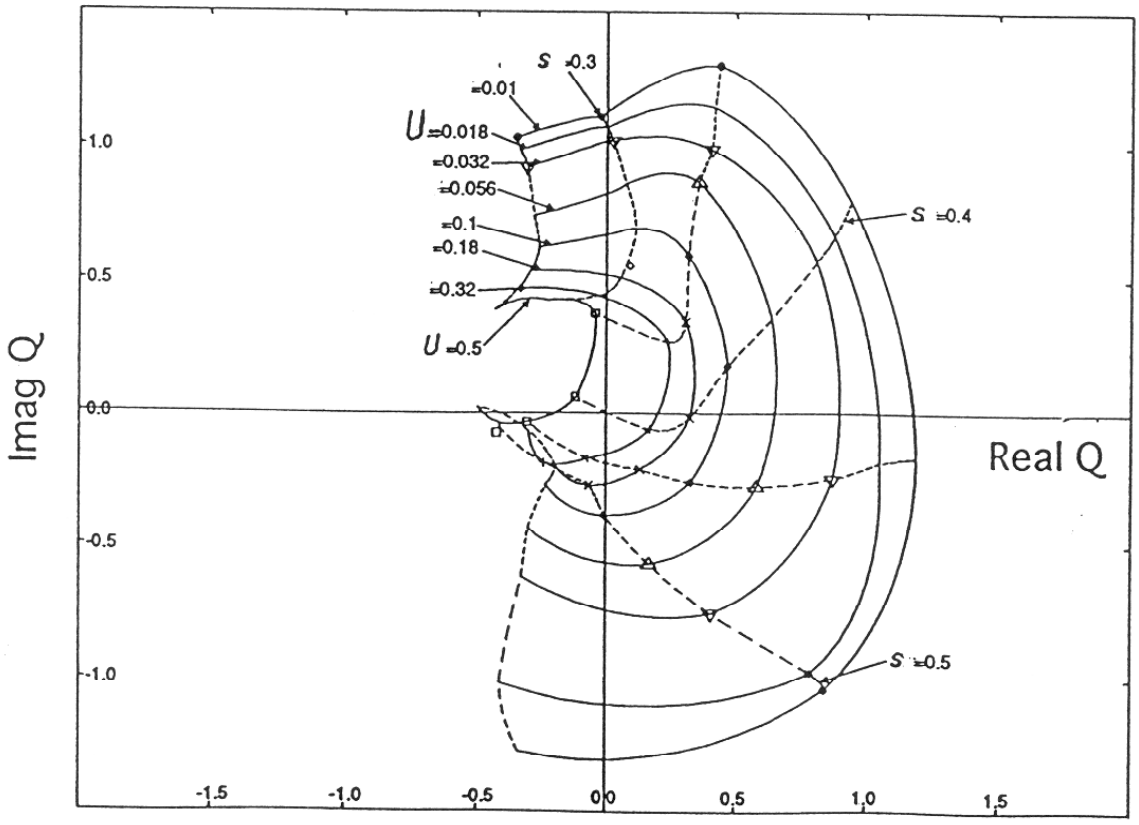

Figure 6.10. Experimentally determined source term Q presented in the complex plane. The level of acoustic pulsation (U = u/V) and the Strouhal number (S = fd/V) are taken as parameters (Graf & Ziada, 1992).

6.4. Counter-measures

6.4.1. Rounding off the branch corners

The effect of rounding the corners at the branch mouth on the fluid resonant mechanism is somewhat complex. Whether it increases or decreases the pulsation amplitude depends on the mode shape of the excited mode, i.e. whether the side branch is coupled with the upstream or the downstream section of the main pipe, see Fig. (6.12). Rounding off the edges affects also the critical flow velocity at which the resonance starts. In the following, these aspects are considered in some detail.

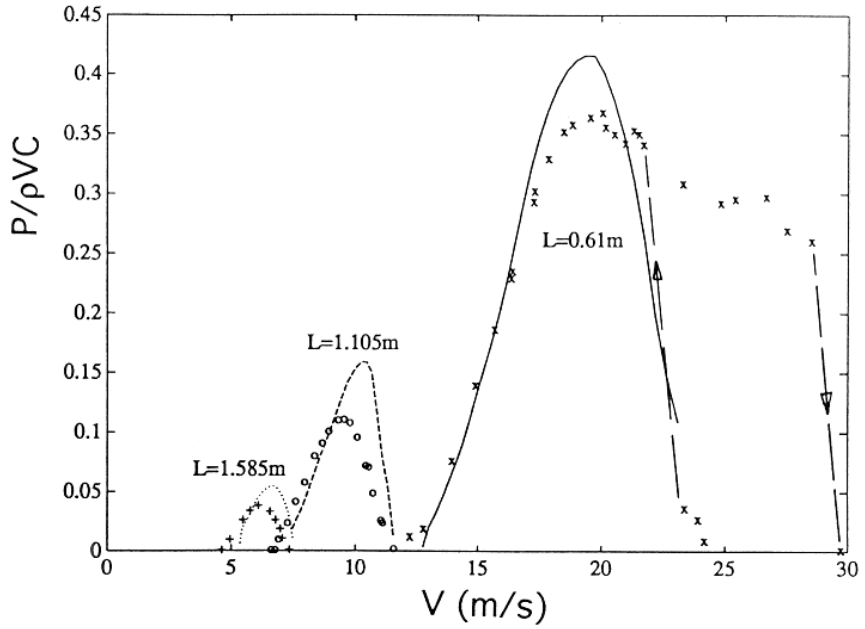

Figure 6.11. Comparison between measured and predicted pulsation amplitude as a function of flow velocity for several cases of symmetric co-axial branches (L_1=L_2= 0.61, 1.105 & 1.585 meter).

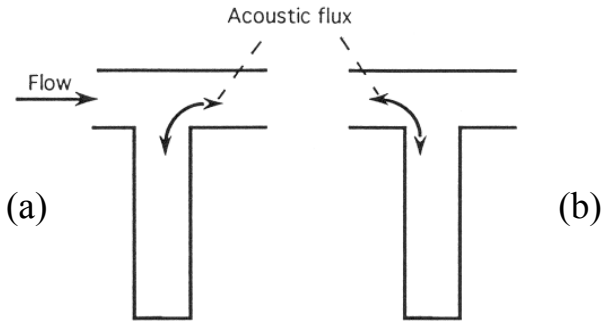

Figure 6.12. Acoustic flux in the T-junction when the branch is coupled with (a) the downstream section and (b) the upstream section of the main pipe.

Figure (6.13) shows the influence of the radius of the branch edge (r) on the acoustic response of a single branch (Bruggeman (1987)). The Strouhal number at resonance becomes independent of r when the branch diameter d is replaced by (d + r), where r is the *radius of the upstream corner.* Thus, rounding the corners, or enlarging the branch diameter at the T-Junction, increases the critical velocity for the onset of resonance, as is already described by Eq. (23).

It can also be seen in Fig. (6.13(a)) that the amplitude of pulsation is decreased by rounding off the edges. This is because the acoustic particle velocity at the branch mouth becomes smaller when the edges are rounded. This feature together with the effect of (r) on the Strouhal number have promoted the general notion that rounding off the edges is, in general, an effective counter-measure. However, Bruggeman (1987) has shown that this is not always the case. In some of his experiments, rounding off the edges increased the pulsation amplitude by a factor of more than 5. It is very helpful therefore, to separate the effect of rounding off the upstream edge from that of the downstream one.

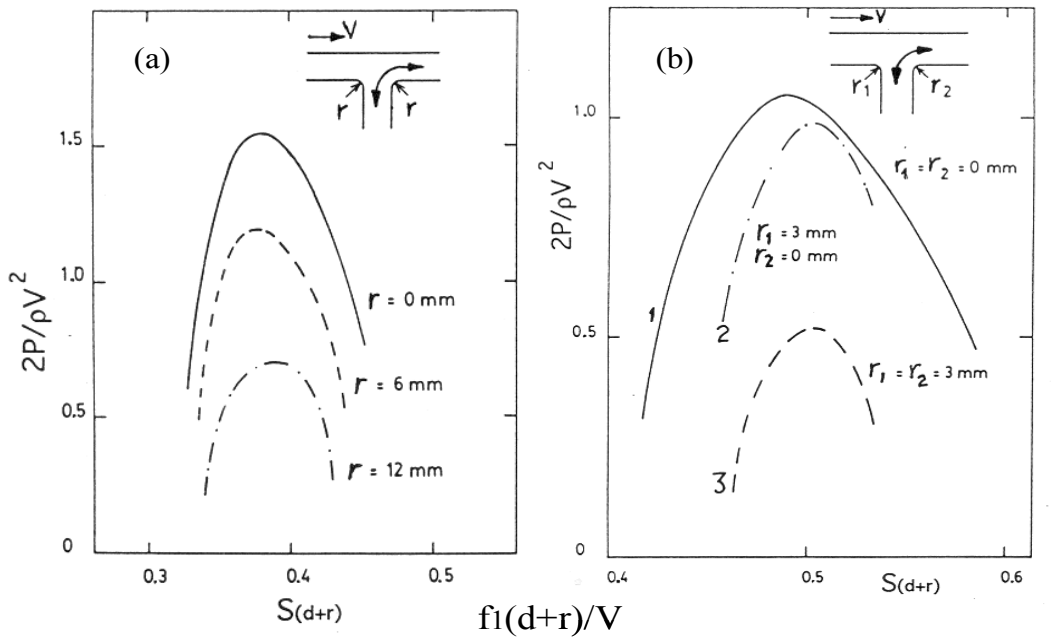

Figure 6.13. Influence of the radius of the branch corners on the amplitude of pulsation. Single branch with square cross-section (Bruggeman, 1987).

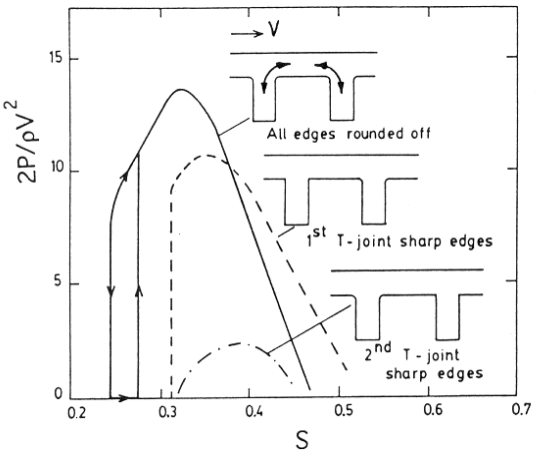

Figure 6.14. Influence of edge radius on pulsation amplitude of two tandem branches (Bruggeman, 1987).

As shown in Fig. (6.13(b)), from Bruggeman (1987), rounding off the upstream edge alone has a negligible effect on the maximum amplitude of pulsation, but rounding off the downstream edge as well reduces substantially the pulsation level. This is because the highest acoustic particle velocity is at the downstream corner, which is due to the fact that the acoustic flux is predominantly between the branch and the downstream section of the main pipe. Rounding this corner therefore reduces the maximum particle velocity and also the acoustic energy produced by its interaction with the shear layer vortices near the downstream corner.

The relationship between the effect of rounding off the edges and the shape of the acoustic mode is well demonstrated in Fig. (6.14). In the case of two tandem branches with $\ell \approx 2L \approx \lambda/2$, the acoustic flux is predominantly in the subsystem consisting of the two branches and the main pipe section between them. Rounding off all edges of the upstream and the downstream branches *increases* the pulsation amplitude! Moreover, the pulsation level is seen to be reduced effectively by

using sharp edges at the mouth of the downstream branch. This is because the sharp upstream edge of the downstream branch increases the local particle velocity, and this increases the sound absorption by the vortex forming at this edge. This phenomenon of sound absorption by vortex shedding from an edge at large amplitude acoustic pulsation is referred to in the literature as "vortex damping" (Bruggeman, 1987; Ziada, 1993).

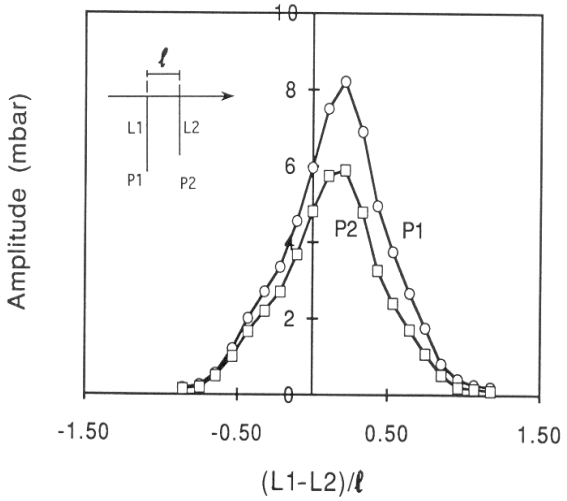

Figure 6.15. Influence of detuning two tandem branches on the maximum amplitude of resonance. ○, Upstream; □, downstream branch.

Figure (6.15) shows test results for the case of tandem branches with $\ell << \lambda/2$. In these tests, the length of one branch was increased in steps while that of the other branch was decreased by an equal amount to keep the frequency of the acoustic mode constant. In this way, the location of the maximum particle velocity, which was initially centred between the side branches, could be shifted towards either branch. Figure (6.15) gives the maximum amplitude at resonance as a function of $\Delta L = L_1 - L_2$. The pulsation level is seen to decrease much faster when the location of the maximum particle velocity becomes closer to the downstream branch (i.e. negative ΔL). Moreover, the pulsation amplitude in the downstream branch is seen to be smaller than that in the upstream branch for all values of ΔL. These results support the supposition of Bruggman (1987) that the attenuation of the pressure pulsation shown in Fig. (6.14) is caused by the increased sound absorption by vortex shedding from the upstream edge of the downstream pipe.

6.4.2. Detuning the branches

As it has been shown already, acoustic resonances of piping systems containing multiple side-branches can be very strong; the pulsation amplitude can exceed the dynamic head in the main pipe by more than one order of magnitude. An effective way to avoid these resonances is to detune the resonance frequencies of the branches, by making one branch shorter (or longer) than the other. For example, in the case of tandem branches shown in Fig. (6.15), the pulsation amplitude becomes negligible when the difference between the lengths of the branches approaches the distance between them, i.e. when $L_1 - L_2 \approx \ell$. It should be noted that it is preferable to make the downward branch longer because the pulsation amplitude decreases faster with ΔL, as is illustrated in Fig. (6.15).

6.4.3. Effect of spoilers

It is well known that shear layer excitation can be weakened by breaking its two-dimensionality in an early stage. This may be achieved by increasing the turbulence level (see the following

section) or adding spoilers near the separation point of the shear layer. The spoilers, also called vortex generators, are surface irregularities introduced to generate three-dimensional disturbances at the initial stage of the instability wave. In this way, the flow development becomes incoherent and the transition to turbulence is accelerated.

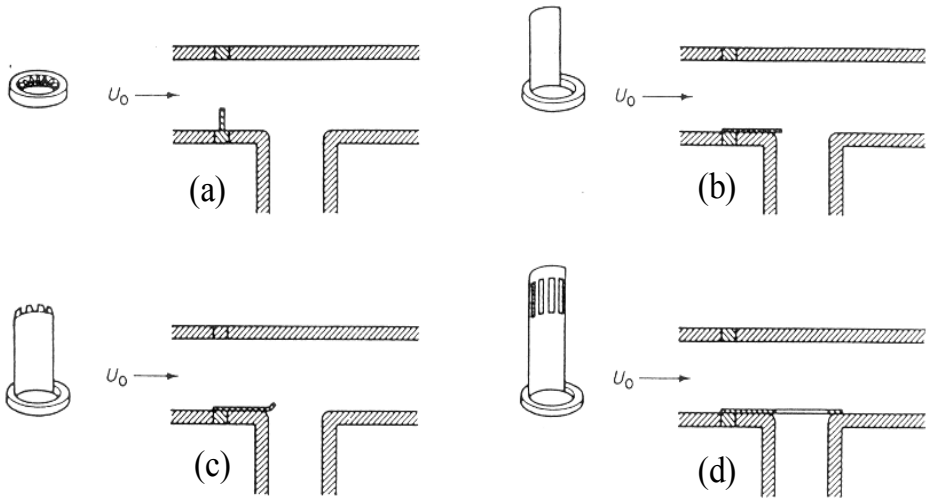

Figure 6.16. Geometry of the spoilers used by Bruggeman et al. (1991) to alleviate the pulsation.

Bruggman et al. (1991) investigated the effect of the spoilers shown in Fig. (6.16). The maximum pulsation amplitudes with and without spoilers are given in Fig. (6.17) as functions of the test pressure. The performance of the spoilers is seen to be pressure dependant, especially when they are placed at the upstream branch. The unsatisfactory performance of the spoilers at high pressures may be attributed to the fact that the scale of turbulence they generate ($\approx 0.1d$) is much smaller than the size of the formed vortices, which scale with the branch diameter d (see Fig. (6.5)). Adding the spoiler on a flat plate (0.1d long) at the downstream branch seems to suppress the resonance for a wide range of test pressures. This is because vortex shedding at this edge is combined with the maximum particle velocity for the fundamental mode of the tandem side-branch resonator. As can be seen from Fig. (6.17), the addition of spoilers at the downstream branches reduces the pulsation amplitude by as much as 30 dB.

6.4.4. Effect of turbulence level

Ziada and Buehlmann (1992) investigated the effect of the turbulence level in the main pipe on the resonance of tandem and co-axial branches. The turbulence was generated by means of an upstream orifice whose diameter was 70% of the main pipe diameter. Varying the distance between the orifice and the branches varied the turbulence level.

As the orifice plate was positioned closer to the branches, the amplitude of the pressure pulsation became smaller, but the resonance peaks became wider. This trend continued until the system response reached its minimum when the orifice was 5.5D upstream. When this distance was further reduced, the pulsation amplitude started to increase again and the resonance peak became much wider, i.e. the pressure pulsations occurred over a wider velocity range. This indicated that the turbulence level produced by the orifice was so high that it excited the system resonance. The system response in this case can be described as a forced response of a resonator (i.e. the side-branches) to broadband turbulence excitation. This phenomenon is referred to in the literature as “turbulent rumble”.

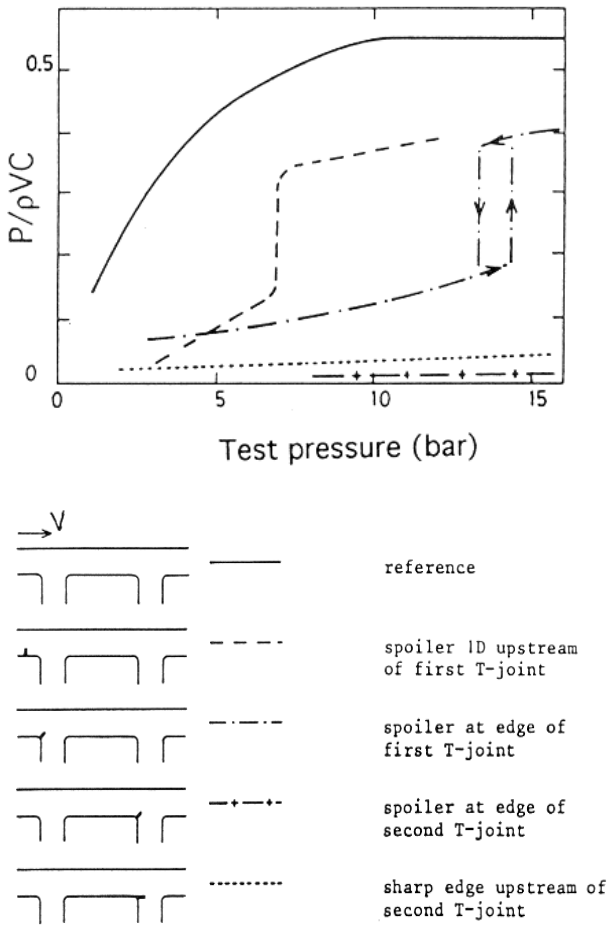

Figure 6.17. Effect of spoilers on the maximum amplitude at the resonance of two tandem branches. The figure shows the effect of the test pressure on the efficiency of spoilers (Bruggeman, 1987).

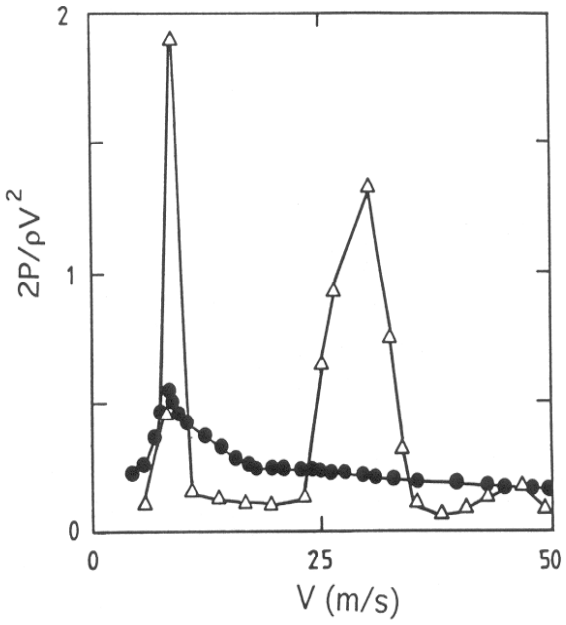

Figure 6.18. Amplitude of pressure pulsation of two tandem branches with and without an orifice plate at 5.5 diameters upstream. Δ, without; ●, with orifice (Ziada & Buehlmann, 1992)

When the orifice is positioned at the optimum location, 5.5D, it reduces the pulsation amplitude by an amount of approximately 12 dB. This is illustrated in Fig. (6.18) for the tandem branches. As mentioned earlier, the orifice should not be positioned too close to the branches; otherwise the turbulence it generates may become an excitation source in itself.

6.4.5. Anti-Vortex Inserts

Jungowski and Studzinski (1989) developed several inserts that can be placed at the mouth of closed side-branches to disturb the process of vortex formation, and thereby dampen the resonance. The geometries of the inserts and how they should be installed at the branch mouth are illustrated in Fig. (6.19). The inserts proved very effective in suppressing the resonance of side-branches. A reduction of up to 40 dB was achieved.

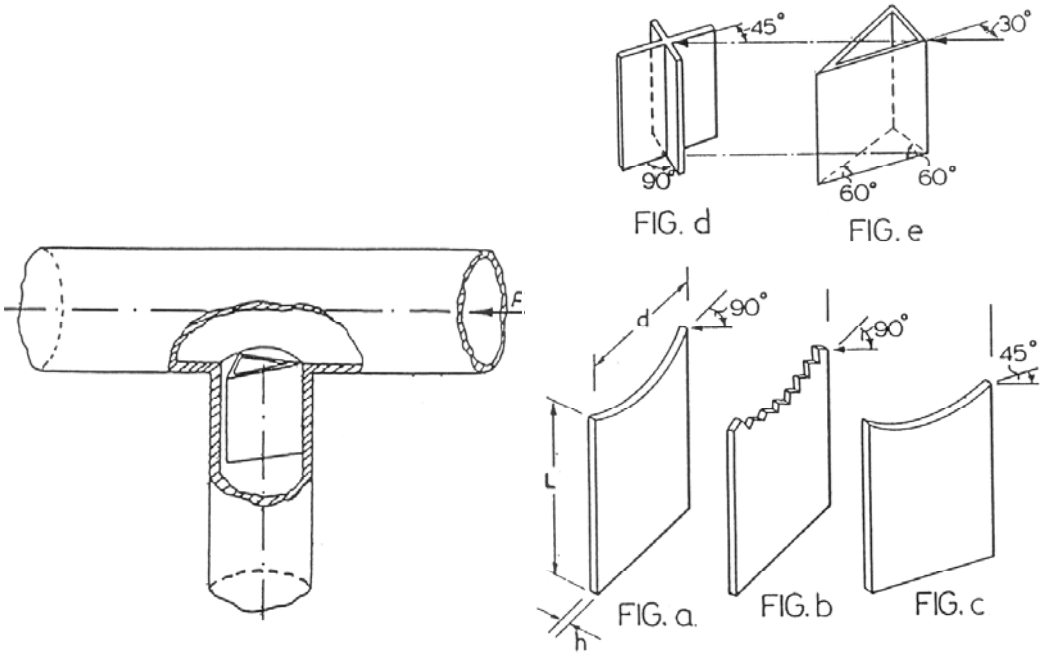

Figure 6.19. Geometries of anti-vortex inserts developed by Jungowski & Studzinki (1989) to dampen flow-excited resonances of side-branches, and a sketch illustrating their positioning at the side-branch mouth.

7. Concluding Remarks

The fluid-dynamic and the fluid-resonant mechanisms have been introduced and discussed for a wide range of flow configurations. The two main events of these mechanisms are the inherent instability of shear flows and the upstream feedback, which is needed to enhance the oscillations at selected frequencies. The first event is reviewed for typical shear flows, such as free shear layers, jets and wakes. Flow impingement, acoustic resonances or structural vibrations generate the upstream feedback. As an example of the fluid-resonant mechanism, the phenomenon of acoustic resonance in closed side-branches is also presented. This example details systematic methods to predict the critical flow velocity for the onset of resonance, to estimate the amplitude of oscillations, as well as to implement reliable counter measures.

The following is a list of selected case histories of industrial problems involving the excitation mechanisms discussed in this paper. References, which describe these cases, are also provided. The list is just a selected collection of the author's industrial experience. Most of these case histories involved measurements in industrial plants and laboratory tests on small-scale models. These model tests were essential in many cases in order to be able to diagnose the excitation mechanism and develop effective counter-measures.

CASE 1: Acoustic resonance in a turbo-compressor (Ziada et al., 2000)

CASE 2: Vibration and noise of a high-pressure by-pass control valve (Ziada et al., 1989)

CASE 3: Vibration and noise of a high-pressure turbine control valve (Ziada et al., 1989)

CASE 4: Acoustic fatigue of a steam piping excited by valve noise (Michaud et al., 2001)

CASE 5: Vibration of a piping system due to flow in a spherical elbow (Ziada et al., 2001)

8. References

Blevins, R.D. 1985 The effect of sound on vortex shedding from cylinders. *Journal of Fluid Mechanics* **161**, 217-237.

Bruggeman, J.C. 1987 *Flow induced pulsation in pipe systems*. Doctoral Dissertation, Eindhoven University of Technology, The Netherlands.

Bruggeman, J.C., Hirsch berg, A., Van Dongen, M.E.H Wijnands,A.P.J & Gorter, J. 1991 Self-sustained aero-acoustic pulsations in gas transport systems:Experimental study of the influence of closed side branches. *Journal of Sound and vibration* **150**, 371-393.

Freymuth, P., 1966, "On Transition in a Separated Laminar Boundary Layer," *Journal of Fluid mechanics* **25**, pp. 683-704.

Graf, H.R. & Ziada, S. 1992 Flow-induced acoustic resonance in closed side branches: An experimental determination of the excitation source. In *Proceedings of ASME International Symposium on Flow-Induced Vibration and Noise, Vol. 7: Fundamental aspects of fluid-structure interactions* (ed M.P. Paidoussis, T. Akylas & P.B. Abraham), AMD-Vol. 51, pp. 63-80, New York: ASME.

Hourigan, K., Welsh, M.C., Thompson, M.C. & Stokes, A.N. 1990 Aerodynamic sources of acoustic resonance in a duct with baffles. *Journal of Fluids & Structures* **4**, 345-370.

Howe, M.S. 1975 Contribution to the theory of aerodynamic sound, with application to excess jet noise and the theory of the flute. *Journal of Fluid mechanics* **71**, 625-673.

Howe, M.S. 1980 The dissipation of sound at an edge. *Journal of Sound and Vibration* **70**, 407-411.

Huerre, P. and Monkewitz, P. 1990 Local and global instabilities in spatially developing flows. *Annual review of Fluid mechanics* **22**, 473-537.

Jungowski, W.M. & Studzinski, W. 1989 Damping pressure pulsations in piping systems. US Patent No. 486 7190

Lucas, M.J., Noreen, R.A., Sutherland, L.C., Cole, J.E. & Junger, M. C. 1977 *Turbomachinery Cavities*, ASME, New York.

Michalke, A. 1965 On spatially growing disturbances in an inviscid shear layer. *Journal of Fluid Mechanics* **23**, 521-544.

Michaud, S., Ziada, S. & Pastorel, H. 2001 Acoustic fatigue of a steam dump pipe system excited by valve noise. *Journal of Pressure Vessel Technology* **16**.

Miksad, R.W. 1972 Experiments on the non-linear stages of free-shear-layer transition," *Journal of Fluid Mechanics* **59**, 695-719.
Naudascher, E. & Rockwell, D. 1994 *flow-induced vibrations: an engineering guide.* Rotterdam: A.A. Balkema, 1994.
Peters, M.C.A.M. 1993 *Aeroacoustic sources in internal flows*. Doctoral Dissertation, Technische Universität Eindhoven, Eindhoven, The Netherlands.
Rockwell, D. & Naudascher, E. 1978 Review-Self sustaining oscillations of flow past cavities. *ASME Journal of Fluids Engineering* **100**, 152-165.
Rockwell, D. and Naudascher, E. 1979 Self-sustained oscillations of impinging free shear layers. *Annual Review of Fluid mechanics* **11**, 67-94.
Stoneman, S.A.T., Hourigan, K., Stokes, A.N. & Welsh, M.C. 1988 Resonant sound caused by flow past two plates in tandem in a duct. *Journal of Fluid Mechanics* **192**, 455-484.
Ziada, S. 1993 Flow-excited resonance of piping systems containing side-branches: Excitation mechanism, counter-measures and design guidelines. International Seminar on Acoustic Pulsations in Rotating Machinary, 1-34, AECL CANDU, Canada.
Ziada, S. 1994 A flow visualisation study of flow-acoustic coupling at the mouth of a resonant side-branch*, Journal of Fluids and Structures* **8**, 391-416.
Ziada, S. 1995 Feedback control of globally unstable flows: Impinging flows. *Journal of Fluids and Structures* **9**, 907-923.
Ziada, S. 2001 Interaction of a jet-slot oscillator with a deep cavity resonator and its control. *Journal of Fluids and Structures* **15**, 831-843.
Ziada, S. & Bühlmann, E.T. 1991 Flow-induced vibration in long corrugated pipes. *Flow Induced Vibrations.* Publication by the Institution of Mechanical Engineers, IMechE 1991-6, 417-426.
Ziada, S. & Bühlmann, E.T. 1992 Self-excited resonances of two side-branches in close proximity. *Journal of Fluids and Structures* **6**, 583-601.
Ziada, S, Bühlmann, E.T. & Bolleter, U. 1989 Flow impingement as an excitation source in control valves. *Journal of Fluids and Structures* **3**, 529-549.
Ziada, S. & Graf, H. 1998 Feedback control of combustion oscillations. *Journal of Fluids and Structures* **12**, 491-507.
Ziada, S., Oengören, A. & Vogel, A. 2000 Flow-excited acoustic resonance in the inlet scroll of a turbocompressor. *Proceedings of the 7th International Conference on Flow-Induced Vibration* (eds. S. Ziada & T. Staubli), Lucerne, Switzerland, June 2000, in press.
Ziada, S. & Rockwell, D. 1982 Self-excited oscillations of a mixing layer-wedge system. *Journal of Fluid Mechanics* **124**, 307-334.
Ziada, S. & Shine, S. 1999 Strouhal numbers of flow-excited acoustic resonance in side branches. *Journal of Fluids and Structures* **13**, 1-16.
Ziada, S., Sperling, H. & Fisker, H. 2001 Vibration of a high-pressure piping system due to flow in a spherical elbow. *Journal of Fluids and Structures* **15**, 751-767.